cells we have observed have abnormal morphologies, such as dispersed chromatin and intact nuclear membranes (Ueno et al., 2002b). Recently, mitotic catastrophe, a type of cell death occurring during or after mitosis with some mitotic failure, has been proposed (Castedo et al., 2004). Although the definition of this cell death yet differs among researchers, 5AzC-induced abnormal mitosis and subsequent apoptosis might fall into this category. Indeed, aberrant entry into mitosis after DNA damage, gene deficiencies, or excess activation of Cdc2-cyclin B1 each suffices to cause mitotic catastrophe (Castedo et al., 2004), which is consistent with our model that includes DNA damage and Cdc2 activation. We should further investigate whether these mitotic cells with abnormal morphology produce two daughter cells with diploid DNA or generate tetraploid G1 cells by mitotic failure; although the results from the BrdU incorporation assay suggest that some of the cells can produce diploid cells (Fig. 3). Regardless, at 9 to 12 h, the amount of activated Cdc2 increased compared with that at 6 h (Fig. 6C), and the number of mitotic cells gradually decreased (Fig. 1B). This pattern suggests that abnormal mitotic entry is suppressed and G2-phase block is induced, although the expression level and phosphorylation state of Chk2, the regulator of the G2 checkpoint after DNA damage, did not change (Fig. 6C). Serum-inducible kinase (Snk/Plk2), which is induced by p53, likely is an inhibitor of mitotic catastrophe (Burns et al., 2003). In our microarray study, we could detect upregulated expression of *Snk/Plk2* at 9 h, when abnormal mitosis began to decrease (Table 1). The mechanism of the G2-phase block is still obscure, but from the study in p53-deficient mice, a p53-independent mechanism may be involved.

Our previous and present results reveal several clues regarding cell cycle and cell death regulation of neural progenitor cells in response to 5AzC-induced stresses, which normally proliferate with a characteristic migration–interkinetic nuclear migration (or "elevator movement")–in the VZ (Takahashi et al., 1995; Fujita, 2003; Fig. 7). Firstly M and secondly G2 progression was blocked from 6 to 9 h after 5AzC treatment and was released thereafter. Delay in inward-migration and accumulation of mitotic cells along the ventricle also were observed (Ueno et al., 2002a,b), which would reflect the delay in cell cycle progression at G2 and M phase. Then, the number of cells in G1 phase and that of apoptotic cells increased. Apoptotic cell death in a p53-dependent way occurred mainly during G1, but also during G2/M and S phase in lesser amounts. Our findings suggest that 5AzC induces apoptosis at multiple cell cycle stages, consistent with the results of another report (Murakami et al., 1995). Together, these results suggest that some cells pass from G2/M to G1 phase with completion of correct DNA repair, others enter G1 but undergo apoptosis because of incomplete repair, and still others stay in G2/M to undergo apoptotic cell death. The upregulated expression of *cyclin B1* and *Cdc20* mRNA at 12 h also suggests that the G2 block was released, and those cells entered G0/G1 phase. The cells dying at G1 after mitosis might have died due to mitotic catastrophe, as a result of incomplete mitosis and faulty DNA repair at G2 or S phase.

Because neural progenitor cells have a high proliferating activity, they are susceptible to many extrinsic stimuli,

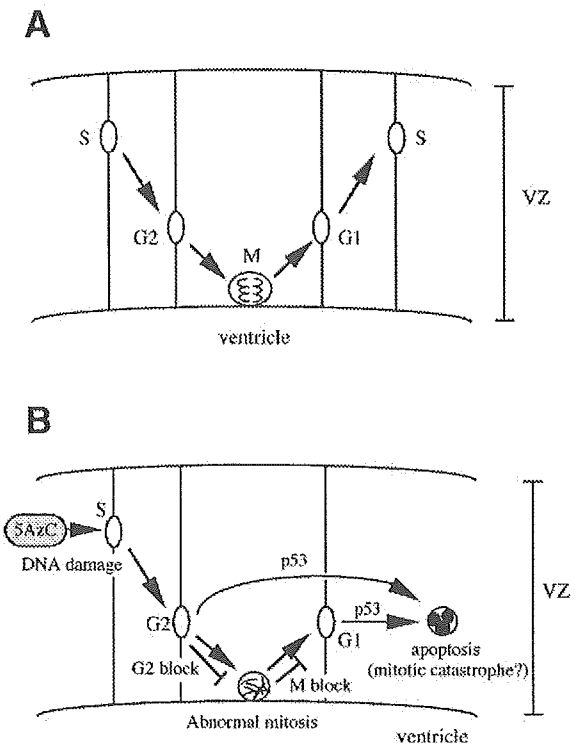

Fig. 7. 5AzC-induced alterations in proliferation of neural progenitor cells. (A) Interkinetic nuclear migration (elevator movement) of neural progenitor cells. Neural progenitor cells proliferate with their nuclei migrating up and down in the VZ. The positions of nuclei are correlated with the cell cycle phases. (B) The schema of the mechanisms of 5AzC-induced cell cycle alteration and apoptosis. 5AzC would be incorporated into DNA in S phase and cause DNA damage. Damaged neural progenitor cells enter M phase with abnormal regulation, such as excess Cdc2 activation, and they accumulate with abnormal morphologies along the ventricle. G2 block also occurs with delay in inward-migration (Ueno et al., 2002a). Then, the cells are divided into daughter cells but undergo apoptosis in G1 phase. G2 phase cells also die by apoptosis. Cell death is induced in a p53-dependent mechanism, but the G2/M phase regulation in a p53-independent way.

especially DNA damage. These cells have the potential to repair after these damages via block of cell cycle progression (or cell cycle arrest) and to exclude highly affected cells through the apoptotic process, although the responses of the cells differ slightly depending on the type of DNA damages. For example, ionizing irradiation induces G1 arrest and apoptosis in neural progenitor cells (Semont et al., 2004), whereas ethylnitrosourea induces S-phase accumulation and apoptosis (Katayama et al., 2005). Regardless, if the adverse extrinsic stimulus is sufficiently low to preclude DNA damage or allow its repair, neural progenitor cells can re-engage and proliferate for correct development of the brain after the injury. However, if the stimulus and subsequent DNA damage are high, excess cell death and cell cycle arrest occur. Thus, once the balance between proliferation and cell death is highly disturbed, it leads to abnormal brain development and results in malformation of the neonatal brain.

Many environmental stresses have a potential to disturb the processes of brain development, i.e. proliferation, migration, and differentiation, however, their mechanisms remain unclear (Rodier, 1995; Mendola et al., 2002; Costa et al., 2004). The

present study revealed how neural cells in the developing brain respond to extrinsic stimuli regarding proliferation and cell death, which offers important information to the mechanisms of fetal brain toxicity induced by widespread environmental stresses. We must further investigate the system the fetal brain uses to repair this damage and the reaction of neural progenitor cells during the repair process.

Acknowledgment

This study was supported financially by the Japan Society for the Promotion of Science.

References

Blaschke, A.J., Staley, K., Chun, J., 1996. Widespread programmed cell death in proliferative and postmitotic regions of the fetal cerebral cortex. Development 122, 1165–1174.

Burns, T.F., Fei, P., Scata, K.A., Dicker, D.T., El-Deiry, W.S., 2003. Silencing of the novel p53 target gene Snk/Plk2 leads to mitotic catastrophe in paclitaxel (taxol)-exposed cells. Mol. Cell. Biol. 23, 5556–5571.

Castedo, M., Perfettini, J.L., Roumier, T., Andreau, K., Medema, R., Kroemer, G., 2004. Cell death by mitotic catastrophe: a molecular definition. Oncogene 23, 2825–2837.

Chaturvedi, P., Eng, W.K., Zhu, Y., Mattern, M.R., Mishra, R., Hurle, M.R., Zhang, X., Annan, R.S., Lu, Q., Faucette, L.F., Scott, G.F., Li, X., Carr, S.A., Johnson, R.K., Winkler, J.D., Zhou, B.B., 1999. Mammalian Chk2 is a downstream effector of the ATM-dependent DNA damage checkpoint pathway. Oncogene 18, 4047–4054.

Costa, L.G., Aschner, M., Vitalone, A., Syversen, T., Soldin, O.P., 2004. Developmental neuropathology of environmental agents. Annu. Rev. Pharmacol. Toxicol. 44, 87–110.

D'Sa, C., Klocke, B.J., Cecconi, F., Lindsten, T., Thompson, C.B., Korsmeyer, S.J., Flavell, R.A., Roth, K.A., 2003. Caspase regulation of genotoxin-induced neural precursor cell death. J. Neurosci. Res. 74, 435–445.

D'Sa-Eipper, C., Roth, K.A., 2000. Caspase regulation of neuronal progenitor cell apoptosis. Dev. Neurosci. 22, 116–124.

Ferguson, A.T., Vertino, P.M., Spitzner, J.R., Baylin, S.B., Muller, M.T., Davidson, N.E., 1997. Role of estrogen receptor gene demethylation and DNA methyltransferase. DNA adduct formation in 5-aza-2′deoxycytidine-induced cytotoxicity in human breast cancer cells. J. Biol. Chem. 272, 32260–32266.

Fujita, S., 2003. The discovery of the matrix cell, the identification of the multipotent neural stem cell and the development of the central nervous system. Cell Struct. Funct. 28, 205–228.

Gao, Y., Sun, Y., Frank, K.M., Dikkes, P., Fujiwara, Y., Seidl, K.J., Sekiguchi, J.M., Rathbun, G.A., Swat, W., Wang, J., Bronson, R.T., Malynn, B.A., Bryans, M., Zhu, C., Chaudhuri, J., Davidson, L., Ferrini, R., Stamato, T., Orkin, S.H., Greenberg, M.E., Alt, F.W., 1998. A critical role for DNA end-joining proteins in both lymphogenesis and neurogenesis. Cell 95, 891–902.

Gorczyca, W., Gong, J., Darzynkiewicz, Z., 1993. Detection of DNA strand breaks in individual apoptotic cells by the in situ terminal deoxynucleotidyl transferase and nick translation assays. Cancer Res. 53, 1945–1951.

Iliakis, G., Wang, Y., Guan, J., Wang, H., 2003. DNA damage checkpoint control in cells exposed to ionizing radiation. Oncogene 22, 5834–5847.

Jackson-Grusby, L., Beard, C., Possemato, R., Tudor, M., Fambrough, D., Csankovszki, G., Dausman, J., Lee, P., Wilson, C., Lander, E., Jaenisch, R., 2001. Loss of genomic methylation causes p53-dependent apoptosis and epigenetic deregulation. Nat. Genet. 27, 31–39.

Juttermann, R., Li, E., Jaenisch, R., 1994. Toxicity of 5-aza-2′-deoxycytidine to mammalian cells is mediated primarily by covalent trapping of DNA methyltransferase rather than DNA demethylation. Proc. Natl. Acad. Sci. U. S. A. 91, 11797–11801.

Karpf, A.R., Moore, B.C., Ririe, T.O., Jones, D.A., 2001. Activation of the p53 DNA damage response pathway after inhibition of DNA methyltransferase by 5-aza-2′-deoxycytidine. Mol. Pharmacol. 59, 751–757.

Katayama, K., Ueno, M., Yamauchi, H., Nagata, T., Nakayama, H., Doi, K., 2005. Ethylnitrosourea induces neural progenitor cell apoptosis after S-phase accumulation in a p53-dependent manner. Neurobiol. Dis. 18, 218–225.

Keramaris, E., Stefanis, L., MacLaurin, J., Harada, N., Takaku, K., Ishikawa, T., Taketo, M.M., Robertson, G.S., Nicholson, D.W., Slack, R.S., Park, D.S., 2000. Involvement of caspase 3 in apoptotic death of cortical neurons evoked by DNA damage. Mol. Cell. Neurosci. 15, 368–379.

Kuida, K., Zheng, T.S., Na, S., Kuan, C., Yang, D., Karasuyama, H., Rakic, P., Flavell, R.A., 1996. Decreased apoptosis in the brain and premature lethality in CPP32-deficient mice. Nature 384, 368–372.

Lakin, N.D., Jackson, S.P., 1999. Regulation of p53 in response to DNA damage. Oncogene 18, 7644–7655.

Liu, Q., Guntuku, S., Cui, X.S., Matsuoka, S., Cortez, D., Tamai, K., Luo, G., Carattini-Rivera, S., DeMayo, F., Bradley, A., Donehower, L.A., Elledge, S.J., 2000. Chk1 is an essential kinase that is regulated by Atr and required for the G(2)/M DNA damage checkpoint. Genes Dev. 14, 1448–1459.

Lu, D.P., Nakayama, H., Shinozuka, J., Uetsuka, K., Taki, R., Doi, K., 1998. 5-Azacytidine-induced apoptosis in the central nervous system of developing rat fetuses. J. Toxicol. Pathol. 11, 133–136.

Matsuoka, S., Rotman, G., Ogawa, A., Shiloh, Y., Tamai, K., Elledge, S.J., 2000. Ataxia telangiectasia-mutated phosphorylates Chk2 in vivo and in vitro. Proc. Natl. Acad. Sci. U. S. A. 97, 10389–10394.

May, P., May, E., 1999. Twenty years of p53 research: structural and functional aspects of the p53 protein. Oncogene 18, 7621–7636.

Mendola, P., Selevan, S.G., Gutter, S., Rice, D., 2002. Environmental factors associated with a spectrum of neurodevelopmental deficits. Ment. Retard. Dev. Disabil. Res. Rev. 8, 188–197.

Michalowsky, L.A., Jones, P.A., 1987. Differential nuclear protein binding to 5-azacytosine-containing DNA as a potential mechanism for 5-aza-2′-deoxycytidine resistance. Mol. Cell. Biol. 7, 3076–3083.

Murakami, T., Li, X., Gong, J., Bhatia, U., Traganos, F., Darzynkiewicz, Z., 1995. Induction of apoptosis by 5-azacytidine: drug concentration-dependent differences in cell cycle specificity. Cancer Res. 55, 3093–3098.

Namihira, M., Nakashima, K., Taga, T., 2004. Developmental stage dependent regulation of DNA methylation and chromatin modification in a immature astrocyte specific gene promoter. FEBS Lett. 572, 184–188.

Nitta, M., Kobayashi, O., Honda, S., Hirota, T., Kuninaka, S., Marumoto, T., Ushio, Y., Saya, H., 2004. Spindle checkpoint function is required for mitotic catastrophe induced by DNA-damaging agents. Oncogene 23, 6548–6558.

Oppenheim, R.W., 1991. Cell death during development of the nervous system. Annu. Rev. Neurosci. 14, 453–501.

Qian, X., Shen, Q., Goderie, S.K., He, W., Capela, A., Davis, A.A., Temple, S., 2000. Timing of CNS cell generation: a programmed sequence of neuron and glial cell production from isolated murine cortical stem cells. Neuron 28, 69–80.

Rao, M.S., 1999. Multipotent and restricted precursors in the central nervous system. Anat. Rec. 257, 137–148.

Rodier, P.M., 1995. Developing brain as a target of toxicity. Environ. Health Perspect. 103, 73–76.

Santi, D.V., Norment, A., Garrett, C.E., 1984. Covalent bond formation between a DNA-cytosine methyltransferase and DNA containing 5-azacytosine. Proc. Natl. Acad. Sci. U. S. A. 81, 6993–6997.

Semont, A., Nowak, E.B., Silva Lages, C., Mathieu, C., Mouthon, M.A., May, E., Allemand, I., Millet, P., Boussin, F.D., 2004. Involvement of p53 and Fas/CD95 in murine neural progenitor cell response to ionizing irradiation. Oncogene 13, 1–12.

Sun, Y.E., Martinowich, K., Ge, W., 2003. Making and repairing the mammalian brain-signaling toward neurogenesis and gliogenesis. Semin. Cell Dev. Biol. 14, 161–168.

Takahashi, T., Nowakowski, R.S., Caviness Jr., 1995. The cell cycle of the pseudostratified ventricular epithelium of the embryonic murine cerebral wall. J. Neurosci. 15, 6046–6057.

Takizawa, T., Nakashima, K., Namihira, M., Ochiai, W., Uemura, A., Yanagisawa, M., Fujita, N., Nakao, M., Taga, T., 2001. DNA methylation is a critical cell-intrinsic determinant of astrocyte differentiation in the fetal brain. Dev. Cell 1, 749–758.

Taylor, W.R., Stark, G.R., 2001. Regulation of the G2/M transition by p53. Oncogene 20, 1803–1815.

Temple, S., 2001. The development of neural stem cells. Nature 414, 112–117.

Thomaidou, D., Mione, M.C., Cavanagh, J.F., Parnavelas, J.G., 1997. Apoptosis and its relation to the cell cycle in the developing cerebral cortex. J. Neurosci. 17, 1075–1085.

Timme, T.L., Thompson, T.C., 1994. Rapid allelotype analysis of p53 knockout mice. Biotechniques 17 (460), 462–463.

Ueno, M., Katayama, K., Nakayama, H., Doi, K., 2002a. Mechanisms of 5-azacytidine (5AzC)-induced toxicity in the rat foetal brain. Int. J. Exp. Pathol. 83, 139–150.

Ueno, M., Katayama, K., Yasoshima, A., Nakayama, H., Doi, K., 2002b. 5-azacytidine (5AzC)-induced histopathological changes in the central nervous system of rat fetuses. Exp. Toxicol. Pathol. 54, 91–96.

Vinson, R.K., Hales, B.F., 2002. DNA repair during organogenesis. Mutat. Res. 509, 79–91.

von Waechter, R., Jaensch, B., 1972. Generation times of the matrix cells during embryonic brain development: an autoradiographic study in rats. Brain Res. 46, 235–250.

Zhu, W.G., Hileman, T., Ke, Y., Wang, P., Lu, S., Duan, W., Dai, Z., Tong, T., Villalona-Calero, M.A., Plass, C., Otterson, G.A., 2004. 5-Aza-2′-deoxycytidine activates the p53/p21Waf1/Cip1 pathway to inhibit cell proliferation. J. Biol. Chem. 279, 15161–15166.

Histol Histopathol (2006) 21: 257-263

http://www.hh.um.es

Histology and Histopathology
Cellular and Molecular Biology

Histopathological changes in the brain of mouse fetuses by etoposide-administration

C. Nam, G.H. Woo, K. Uetsuka, H. Nakayama and K. Doi
Department of Veterinary Pathology, Graduate School of Agricultural and Life Sciences, The University of Tokyo, Bunkyo-ku, Tokyo, Japan

Summary. Etoposide (VP-16), a topoisomerase II inhibitor, is an anti-tumor agent which is also known to show embryotoxicity, and teratogenicity when administered to pregnant rodents. We examined VP-16-induced histopathological changes in the brain of mouse fetuses. Pregnant mice were intraperitoneally injected with VP-16 (4 mg/kg) on day 12 of gestation (GD 12), and fetuses were collected from 1 to 48 hours after treatment (HAT). Mitotic neuroepithelial cells in the telencephalic wall prominently decreased at 2 HAT, and were hardly observed at 4 HAT. The number of pyknotic neuroepithelial cells in the fetal brain began to increase at 4 HAT, and became prominent from 8 to 24 HAT. These pyknotic cells were also positively stained by TUNEL method, which can detect fragmented DNA, and showed ultrastructural characteristics of apoptosis. Additionally, these cells were also positive for cleaved caspase-3, an essential executioner of apoptosis. This indicated that excessive neuroepithelial cell apoptosis was induced in the brain of mouse fetuses following VP-16 treatment on GD 12.

Key words: Apoptosis, Brain, Etoposide, Fetus, Mouse

Introduction

Epotoside (VP-16) is a semisynthetic derivative of podophyllotoxin, which is extracted from a plant *Podophyllum peltatum* and has an antitumor activity (Sieber et al., 1978). VP-16 is widely used as an anticancer chemotherapeutic agent for small cell lung cancer, testicular cancers and lymphomas (Hande, 1998). VP-16, a topoisomerase II inhibitor, impairs DNA synthesis by forming complexes with the cleaved DNA and prevents relegation of the double-strand breaks in the replicating cells (Chen and Liu, 1994). On the other hand, VP-16 is embryocidal and teratogenic in rats and mice. For example, a single intraperitoneal injection of VP-16 to pregnant mice on day 6, 7, or 8 of gestation (GD 6, 7 or 8) caused embryotoxicity, cranial abnormality, and major skeletal malformation (Sieber et al., 1978).

However, details of histopathological changes were not investigated in the brain of fetuses following VP-16 administration to their dams. Therefore, we carried out detailed histopathological examination on the fetal brain obtained from pregnant mice which were treated with VP-16 on GD 12.

Offprint request to: Dr. Chunja Nam, Department of Veterinary Pathology, Graduate School of Agricultural and Life Sciences, The University of Tokyo, 1-1-1 Yayoi, Bunkyo-ku, Tokyo 113-8657, Japan. e-mail: vet0215@yahoo.co.kr

Materials and methods

Animals and treatments

Eight-week-old pregnant ICR (Crj:CD-1) mice were obtained from Charles River Japan Co., Yokohama, Japan. Mice were kept using an isolator caging system (Niki Shoji Co., Tokyo) under controlled conditions (23±2°C with 55±5% humidity and a 14-hr light/10-hr dark cycle) and fed commercial pellets (MF, Oriental Yeast Co., Ltd., Tokyo) and tap water ad libitum. VP-16 (Sigma, St. Louis, MO) was first dissolved in 1% dimethyl sulphoxide (DMSO) solution in physiologic saline.

Thirty-five 8-week-old pregnant mice were injected with 4 mg/kg of VP-16 intraperitonially (i.p.) on GD 12, and each group including five dams were sacrificed by exsanguinations under ether anesthesia at 1, 2, 4, 8, 12, 24, and 48 hours after treatment (HAT), respectively. Twenty-one age-matched pregnant mice were injected i.p. with 1% DMSO solution on GD 12, and three dams were sacrificed in the same way at 1, 2, 4, 8, 12, 24, and 48 HAT, respectively. Fetuses were collected by Caesarian section from dams.

The protocol of the present study was approved by

the Animal Use and Care Committee of the Graduated School of Agricultural and Life Sciences, the University of Tokyo.

Histopathology

The fetuses obtained from the dams as scheduled were fixed in 10% neutral-buffered formalin and embedded in paraffin. Four-μm paraffin sections were then stained with hematoxylin and eosin (HE) for histopathological examination.

Immunohistochemistry

Immunohistochemical staining was carried out by LSAB method. Anti-cleaved caspase-3 antibody was obtained from Cell Signaling Technology., USA, and anti-proliferating cell nuclear antigen (PCNA) antibody was purchased from Novacostra Laboratories, UK. Paraffin sections were deparaffinized and immersed in 10mM citrate buffer, pH 6.0, and autoclaved for 10 min at 121°C. After washing in Tris-buffered saline (TBS), the sections were placed in 0.3% H_2O_2-containing methanol for 30 min to inactivate endogenous peroxidase. After incubation in skimmed milk at 37°C for 40 min to reduce non-specific staining, the sections were reacted with primary antibodies at 4°C overnight, with secondary antibody at room temperature for 40 min, and then with peroxidase-labeled streptoavidine (Dako, CA) at room temperature for 40 min, respectively. The sections were visualized by peroxidase-diaminobenzidine (DAB) reaction and then counterstained with methyl green.

In situ detection of fragmented DNA (apoptosis)

DNA fragmentation was examined on the paraffin sections by a modified TUNEL (Terminal deoxynucleotidyl Transferase Biotin-dUTP Nick End Labeling) method, which was first proposed by Gavrieli et al. (1992) and has been widely used for the detection of apoptotic cells. A commercial apoptosis detection kit (ApopTag® Peroxidase *In situ* Apoptosis Detection Kit; Chemicon, CA) was used in the present study. In brief, multiple fragmented DNA 3'-OH ends on a deparaffinized section were labeled with digoxigenin-dUTP in the presence of terminal deoxynucleotidyl transferase (TdT). Peroxidase-conjugated anti-digoxigenin antibody was then reacted with the section. Apoptotic nuclei were visualized by diaminobenzidine (DAB) reaction. The sections were then counterstained with methyl green.

Electron microscopy

Some fetal brain tissues were subjected to electron microscopic examination. Small pieces of the tissues were fixed in 2% glutaraldehyde in 0.1M phosphate buffer (pH 7.4), postfixed in 1% osmium tetroxide in the same buffer, and embedded in an epoxy resin (Oken, Shoji Co., Tokyo). Semithin sections were stained with toluidine blue for light microscopic survey. Ultrathin sections of selected areas were then double-stained with uranyl acetate and lead citrate, and observed using a JOEL 1200 EX electron microscope (Nippon Denshi Co., Ltd., Tokyo).

Cell counting

The number of mitotic cells in the ventricular zone (VZ) of telencephalon, was counted on one HE-stained section each for randomly chosen two fetuses per dam. TUNEL-positive and cleaved caspase-3-positive neuroepithelial cells in the telencephalon were counted on one immunostained section each for six fetuses per dam. One thousand cells were counted on each section under a light microscope (X400). Values were expressed as mean ± standard deviation (SD) at each point of examination, and statistical analysis was done by Student's t-test.

Results

There were no significant differences in body weight changes of fetuses between the VP-treated and control groups.

VP-16 administration induced histopathological changes in the fetal brain. Mitotic-index of neuroepithelial cells of the telencephalon began to decrease significantly at 2 and 4 HAT, and then recovered to the control level at 8 HAT (Fig. 1). At 4 HAT, there were only few mitotic neuroepithelial cells in the VZ of telencephalon.

Pyknotic cells in the telencephalon of VP-16 treated mice began to increase at 4 HAT, peaked at 12 HAT, gradually decreased at 24 HAT, and then returned to the control level at 48 HAT (Fig. 2). Pyknotic cells in the

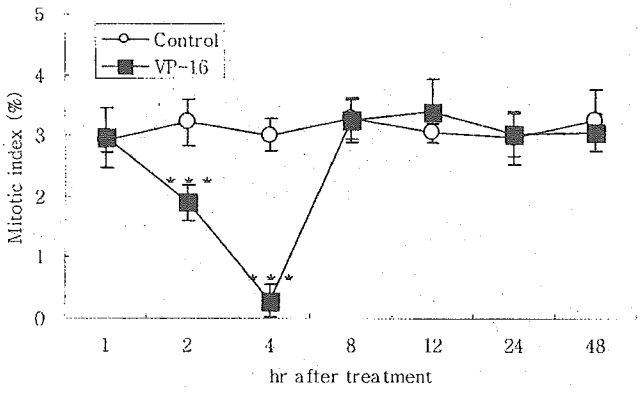

Fig. 1. Changes in the mitotic index (%) in the telencephalic wall of the fetal brain. Each value represents the mean ± SD of 2 fetuses obtained from each dam. ***p<0.001: Significantly different from control.

telencephalon were observed mainly in the ventral layer at 4 HAT and mainly in the middle and dorsal layers of the VZ at 8, 12, and 24 HAT, respectively (Fig. 2). Futhermore, in some fetuses, neuroepithelial cell arrangement was affected by the loss of pyknotic cells. These cells fell into the ventricular apace at 12 and 24 HAT.

Almost all of the pyknotic cells in the VP-16 treated fetal tissues were positive for TUNEL and cleaved caspase-3 (Figs. 3, 5). The time course of the number of TUNEL-positive cells in the telencephalic wall corresponded well to that of pyknotic cells. The number of TUNEL-positive cells increased significantly from 8 HAT, reached the peak at 12 HAT, decreased at 24 HAT, and then returned to the control level at 48 HAT (Fig. 4). Only a few TUNEL-positive cells were observed in controls. Cleaved caspase-3-positive cells in the VZ increased moderately at 4 HAT, peaked at 8 and 12 HAT, and decreased at 24 HAT (Fig. 6). On the other hand, PCNA-positive cells in the VZ slightly decreased only at 12 HAT compared to controls.

Electron-microscopically, the pyknotic cells were characterized by shrinkage of the cell body, condensation of nuclear chromatin and margination of condensed chromatin along the nuclear membrane (Fig 7a). Some apoptotic cells were fragmented into small pieces, which were frequently ingested by adjacent cells and macrophages (Fig 7b).

A similar but less prominent pyknotic changes were also observed in the diencephalon, mesencephalon, metencepahlon, spinal cord (only near the spinal canal area), and mesenchyme of limbs in VP-16-treated fetuses. Almost of these cells were also positive for TUNEL and cleaved caspase-3.

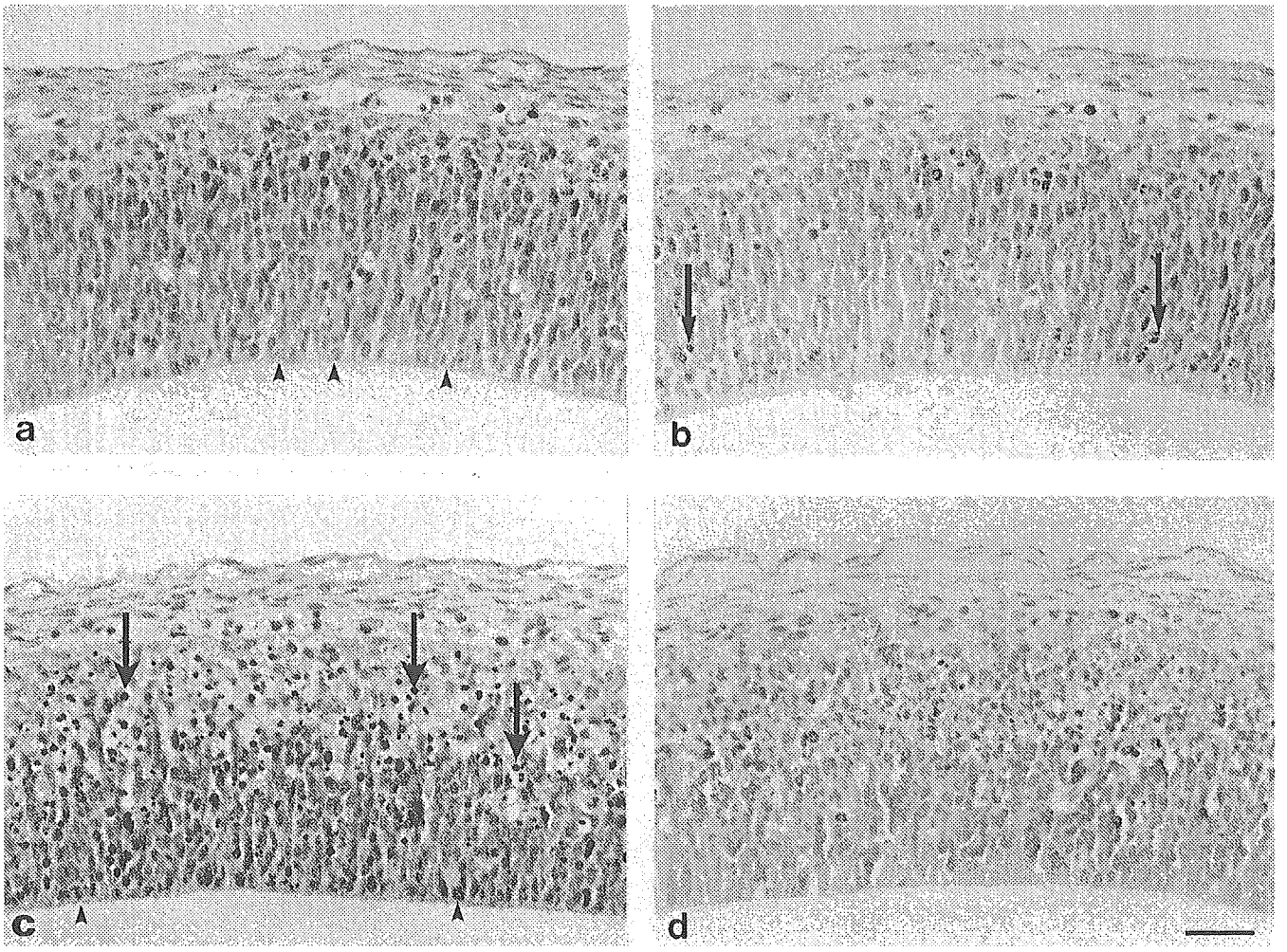

Fig. 2. Histological appearances of the telencephalic wall of a control fetus **(a)** and those of VP-16-treated fetuses at 4 HAT **(b)**, 12 HAT **(c)**, and 24 HAT **(d)**. HE stain, bar: 31 μm. Pyknotic cells were observed from 4 HAT. The number of pyknotic cells peaked at 12 HAT, and then gradually decreased at 24 HAT. Arrowheads: mitotic cell; Arrows: pyknotic cell. x 400

Discussion

Etoposide (VP-16), a topoisomerase II inhibitor, has been widely used as an antitumor drug since 1970. VP-16 is also known as a genotoxic and teratogenic chemical. This study was focused on morphological characteristics of the fetal mouse brain lesions treated with VP-16 on GD 12.

Almost all of the nuclei of VP-16-induced pyknotic cells were positive for TUNEL stain and cleaved caspase-3. Activation of caspase-3 is an essential event for apoptosis, and it is either partially or totally responsible for the proteolytic cleavage of many key proteins during the apoptotic cascade such as the nuclear enzyme poly (ADP-ribose) polymerase (PARP) (Fernandes-Alnemri et al., 1994). Moreover, electron microscopic features of these cells accorded well with the ultrastructural characteristics of apoptotic cells (Ihara et al., 1998). TUNEL method, which can detect fragmented DNA *in situ*, is widely used for the evaluation of apoptotic cells. Even though some researchers have recently demonstrated that TUNEL technique may not be specific for apoptotic cells, and it also detects a small population of necrotic cells (de Torres et al., 1997; Levin et al., 1999), the detection of cleaved caspase-3 and ultrastructural morphology in the VP-16-treated fetal mouse brain in this study verified apoptotic changes. Therefore, it is reasonable to consider that the pyknotic cells observed in the fetal brain of the VP-16-treated fetuses are apoptotic ones.

Following VP-16 treatment to pregnant mice on GD 12, a marked decrease of mitosis of neuroepithial cells was observed in the VZ from 2 HAT to 4 HAT. The cleaved caspase-3-positive cells began to increase at 4 HAT, peaked at 8 and 12 HAT, and then decreased weakly at 24 HAT. This indicates that VP-16-induced apoptotic changes of neuroepithelial cells began to occur at 4 HAT. Decreased mitotic index before apoptotic

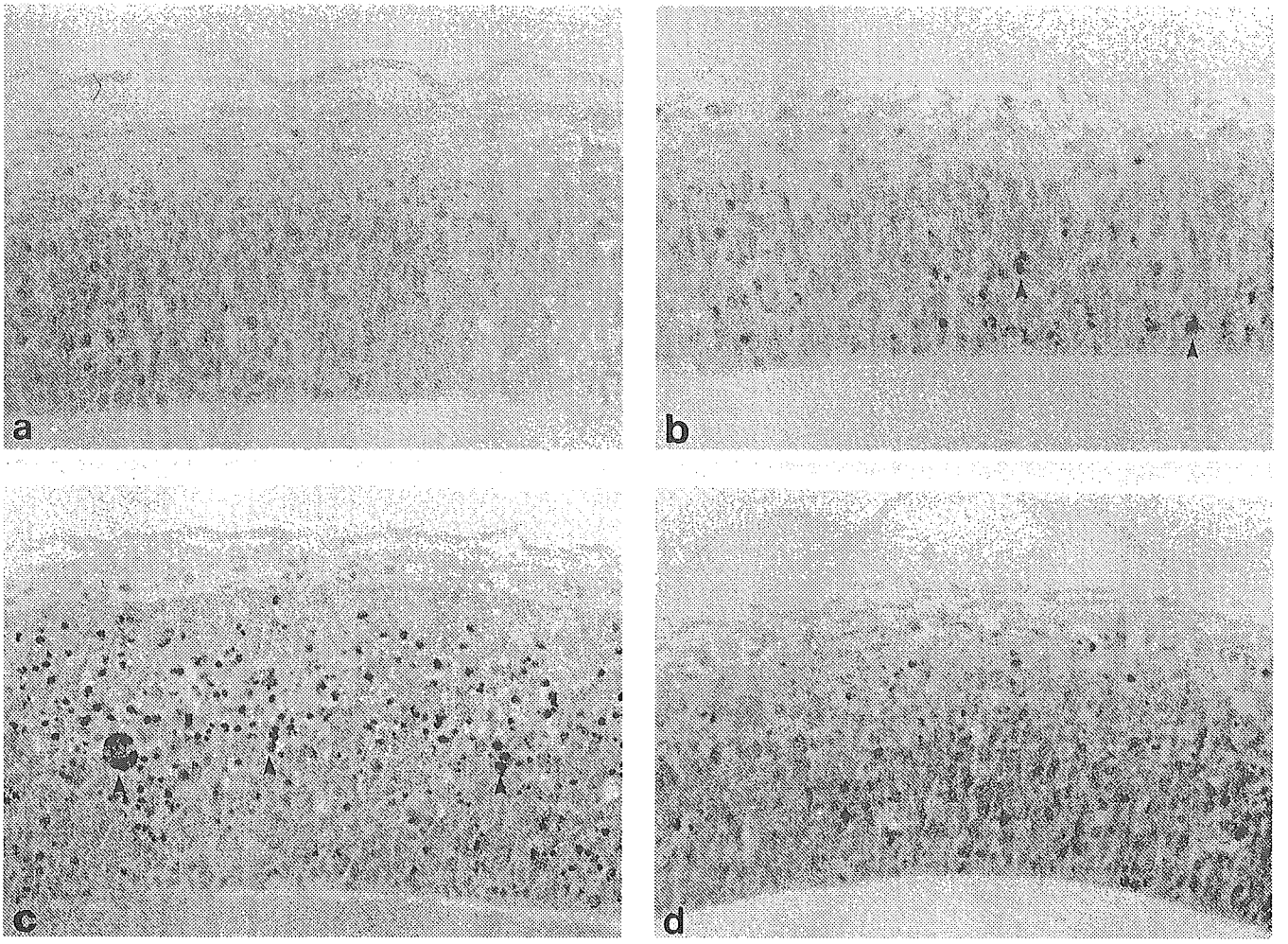

Fig. 3. TUNEL-positive cells in the telencephalic wall of the fetal brain of a control **(a)** and those of VP-16-treated fetuses at 4 HAT **(b)**, 12 HAT **(c)**, and 24 HAT **(d)**. The number of TUNEL-positive cells began to increase from 4 HAT, peaked at 12 HAT, and decreased at 24 HAT. Arrowheads: TUNEL-positive cells. x 400

changes demonstrated in the present study suggested that the initiation of neuroepithelial damage might occur in the pre-mitotic phase of the cell cycle. Apoptotic neuroepithelial cells were mainly observed in the middle and dorsal layers of the VZ at 8, 12, and 24 HAT. It is reported that the neuroepithelial cells in the dorsal layer actively synthesize DNA (S-phase), and those of the middle layer are in the G1 or G2 phase of the cell cycle (Langman et al., 1966). VP-16 has also been reported to induce apoptosis throughout late G1/S or G1 arrest in mouse embryo fibroblasts (Attardi et al., 2004).

Apoptotic changes in neuroepithelial cells of the fetal brain were reported in rats and mice following prenatal treatment with other teratogenic drugs such as 5-azacytidine (Lu et al., 1998), ethylnitrosourea (Katayama et al., 2000), hydroxyurea (Woo et al., 2003), and 1-ß-arabinofuranosylcytosine (Yamauchi et al, 2003). The present study showed that VP-16 can also

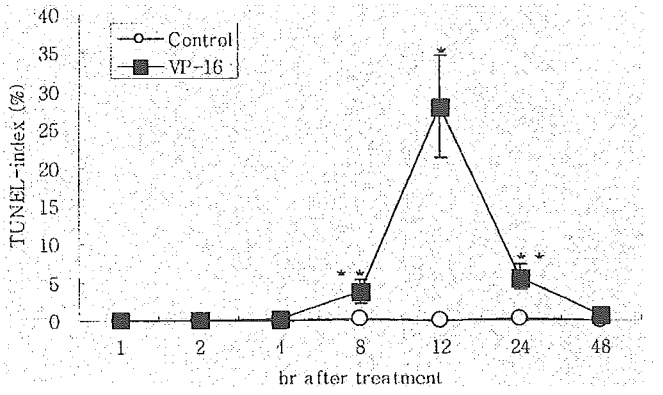

Fig. 4. Changes in the TUNEL-index (%) in the telencephalic wall of the fetal brain. Each value represents the mean ± SD of 6 fetuses obtained from each dam. *p<0.05: Significantly different from controls, **p<0.01: significantly different from controls.

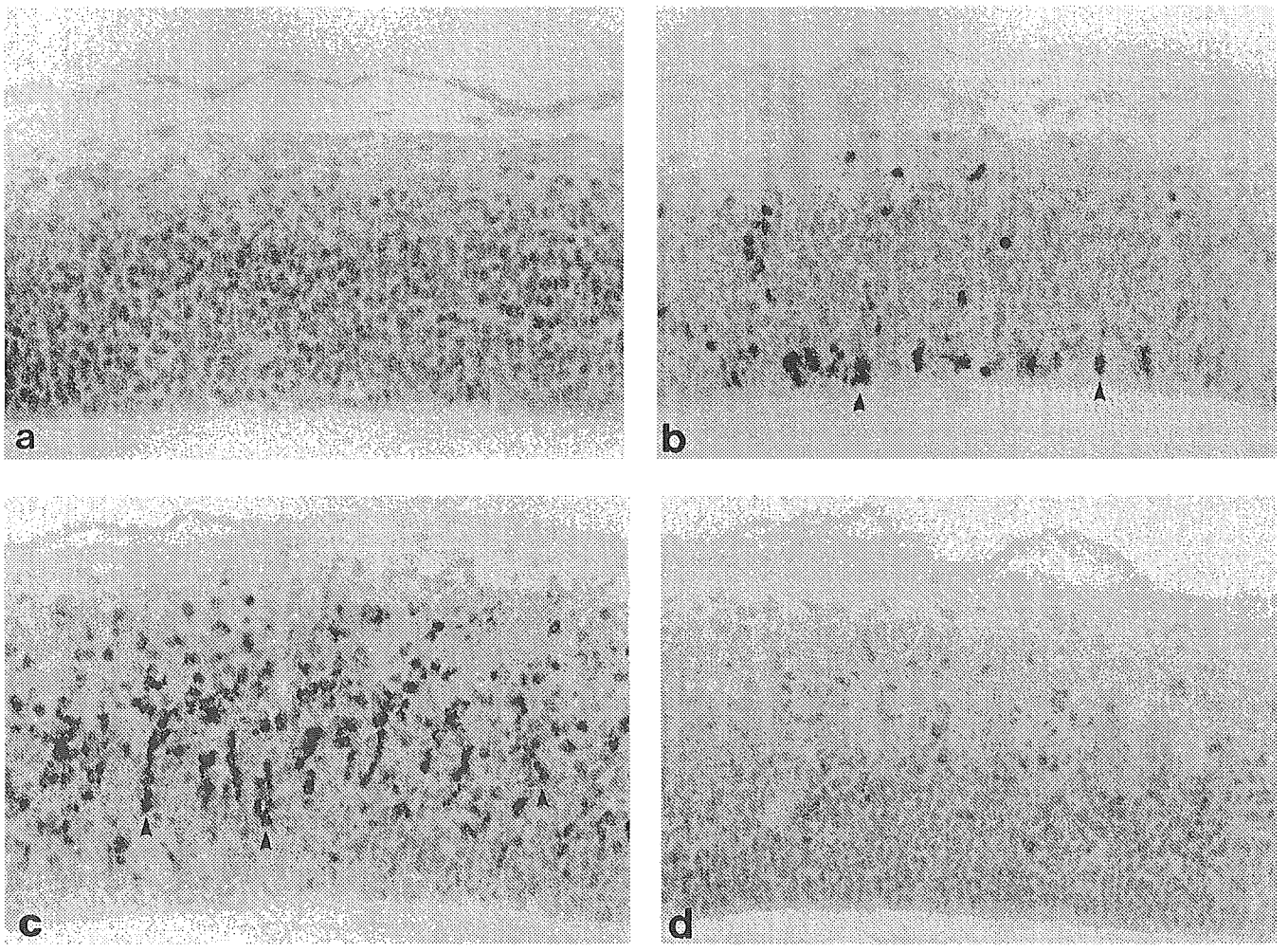

Fig. 5. Immunostaining for cleaved caspase-3 in the telencephalic wall of a control fetus **(a)** and of VP-16-treated fetuses at 4 HAT **(b)**, 12 HAT **(c)**, and 24 HAT **(d)**. The cleaved caspase-3 positive cells began to increase at 4 HAT, peaked at 8 and 12 HAT, and decreased at 24 HAT. Arrowheads: cleaved caspase-3-positive cell. x 400

induce similar morphological changes in the fetal brain. These findings suggest that the fetal brain in the organogensis phase might be very sensitive to such teratogenic chemical exposures.

VP-16 alters microtubule assembly, and mainly poisons topoisomerase II by increasing the steady-state concentrate of their covalent DNA cleavage complexes. Therefore this action converts topoisomerases into physiological toxins that cause high levels of transcript of transient-associated DNA breaks in the genome (Chen and Liu, 1994; Jesen and Sehested, 1997; Hande, 1998). When VP-16 was removed, DNA breakage was quickly repaired (Wozniak and Ross, 1983; Hande, 1998). Plasma half –life of VP-16 is less than 2 hr in mice when injected i.p. and 6.4 hr in human via intravenous route (Dorr et al., 1989; Hande, 1998). According to our present results, rapid recovery from VP-16-induced cellular damage caused by VP-16 corresponded well to the pharmacokinetics of VP-16.

Single injection of VP-16 (1.5, 2, and 3 mg/kg) at the early gestation period caused embryocidal or more severe teratogenic effects such as major skeletal malformation and/or various cranial abnormalities (Sieber et al., 1978). In the present study, administration of VP-16 of 4 mg/kg to pregnant mice on GD 12 (fetal organogenesis phase) induced apoptotic cell death only in the fetal CNS and mesenchyme of limbs. Accordingly, VP-16 administration into dams might induce various embryotoxic and teratotoxic effects, depending on the

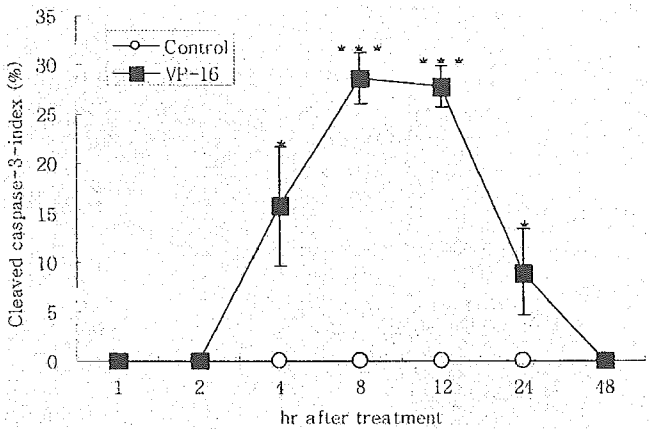

Fig. 6. Changes in the cleaved caspase-3-index (%) in the telencephalic wall of the fetal brain. Each value represents the mean ± SD of 6 fetuses obtained from each dam. *p<0.05: significantly different from control, ***p<0.001: significantly different from control.

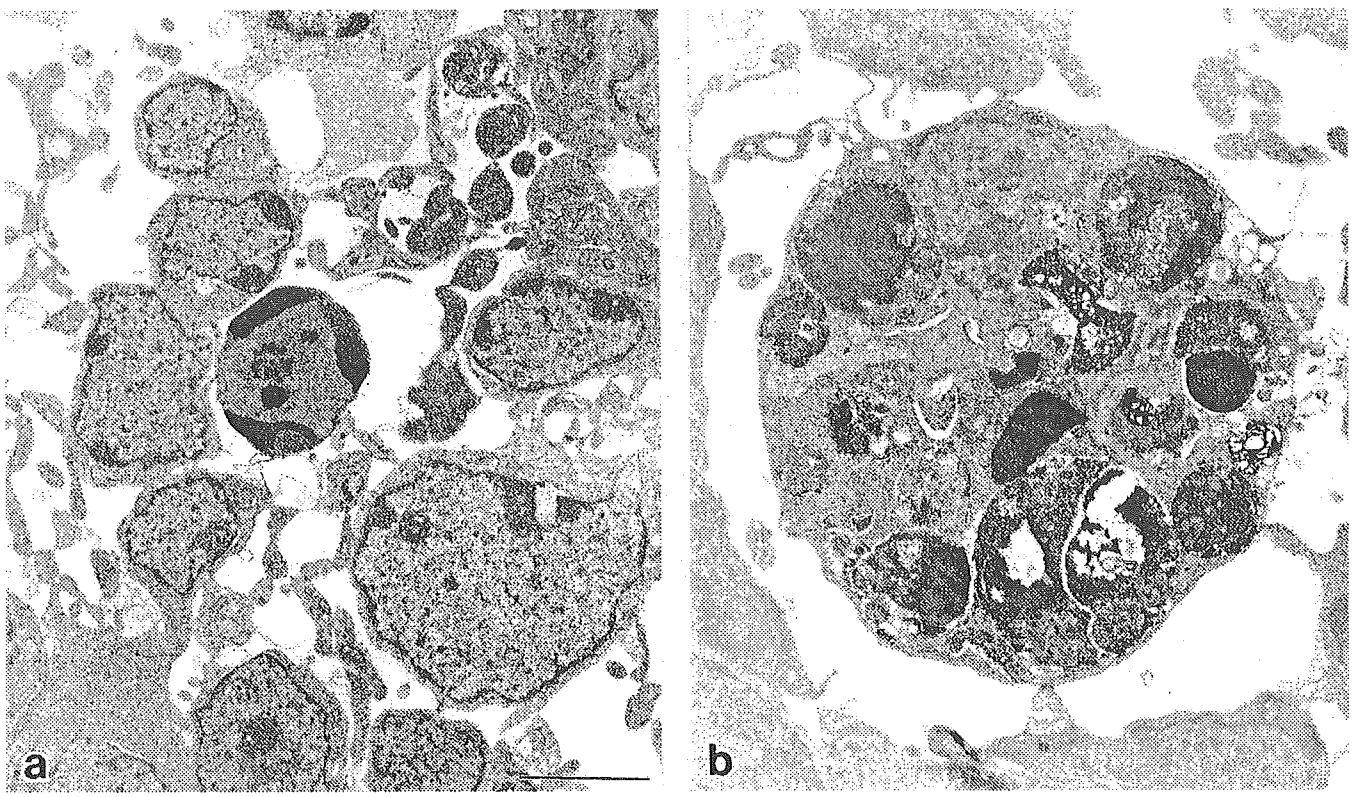

Fig 7. Electron microscopy of the telencenphalic wall of the VP-16-treated mouse fetal brain. **a.** An apoptotic cell at the center shows margination of condensed nuclear chromatin along the nuclear membrane. **b.** Apoptotic bodies are ingested by a macrophage. Bar: 2.0 μm.

gestational day of VP-16 injection.

In conclusion, cellular damage in the fetal brain obtained from pregnant mice treated with VP-16 on GD 12 was apoptotic cell death. The present results offer a clue for studies on the mechanisms of fetotoxicity and teratogenicity induced by VP-16. Further studies on gene expression profiles are now in progress in the fetal brain after VP-16 administration to dams.

Aknowledgements. The authors appreciate Akira Yososhima, Department of Veterinay Pathology, the University of Tokyo, for his excellent technical assistant for electronmicroscopy.

References

Attardi L.D., Vries A. and Jacks T. (2004). Activation of the p53-dependent G1 checkpoint response in mouse embryo fibroblasts depends on the specific DNA damage inducer. Oncogene 23, 973-980.

Chen A.Y. and Liu L.F. (1994). DNA topoisomerases: essential enzymes and lethal targets. Annu. Rev. Pharmacol. Toxicol. 34, 191-218.

de Torres C., Munell F., Ferrer I., Reventos J. and Macaya A. (1997). Identification of necrotic cell death by the TUNEL assay in the hypoxic-ischemic neonatal brain. Neurosci. Lett. 230, 1-4.

Dorr R.T., Liddil J.D., von Hoff D.D., Sobe M. and Osborne C.K. (1989). Antitumor activity and murine pharmacokinetics of paraental acronycine. Cancer Res. 49, 340-344.

Fernandes-Alnemri T., Litwack G.. and Alnemri G.S. (1994). CPP32, a novel human apoptotic protein with homology to Caenorhabditis elegans cell death protein Ced-3 and mammalian interleukin-1 beta-converting enzyme, J. Biol. Chem. 269, 30761-30764.

Gavrieli Y., Sherman Y. and Ben-Sasson S.A. (1992). Identification of programmed cell death in situ via specific labeling of nuclear DNA fragment. J. Cell Biol. 119, 493-501.

Hande K.R. (1998). Etoposide: four decades of development of topoisomerase inhibitor. Eur. J. Cancer 34, 1514-1521.

Ihara T., Yamamoto T., Sugamata M., Okumura H. and Ueno Y. (1998). The progress of ultrastuctural changes from nuclei to apoptotic body. Virchows Arch. 433, 443-447.

Jensen P.B. and Sehested M. (1997). DNA topoisomerase II rescued by catalytic inhibitors: a new strategy to improve the antitumor selectivity of etoposide. Biochem. Pharmacol. 54, 755-759.

Katayama K., Ishigami N., Uetsuka K., Nakayama H. and Doi K. (2000). Ethylnitrourea (ENU)-induced apoptosis in the fetal tissues. Histol. Histopathol. 15, 707-711.

Langman J., Guerrant R.L. and Freeban B.G. (1966). Behavior of neuroepithelial cells during closure of the neural tube. J. Comp. Neurol. 132, 355-374.

Levin S., Bucci T.J., Cohen S.M., Fix A.S., Hardisty J.F., LeGrand E.K., Maronpot P.R. and Trump B.F. (1999). The nomenclature of cell death: Recommendation of an ad hoc committee of the society of toxicological pathologists. Toxicol. Pathol. 27, 484-490.

Lu D.P., Nakayama H., Sinozuka J., Uetsuka K., Taki R. and Doi K. (1998). 5-Azacytidine-induced apoptosis in the central nervous system of developing rat fetuses. J. Toxicol. Pathol. 11, 133-136.

Sieber S.M., Whang-Peng J., Botkin C. and Knutsen T. (1978). Teratogenic and cytogenetic effects of some plant-derived antitumor agents (vincristine, colochicine, maytasine, VP-16-213 and VM-216) in mic. Teratology 18, 31-48.

Woo G.H., Katayama K., Jung J.Y., Uetsuka K., Bak E.J., Nakayama H. and Doi K. (2003). Hydroxyurea (HU)-induced apoptosis in the mouse fetal tissues. Histol. Histopathol. 15, 387-392.

Wozniak A.J. and Ross W.E. (1983). DNA damages a basis for 4-demethyl-epipodophyllotoxicity. Cancer Res. 43, 120-124

Yamauchi H., Katayama K., Yososhima A., Uetsuka K., Nakayama H. and Doi K. (2003). 1-ß-Arabinofuranosylcytosine(Ara-C)-induced apoptosis in the rat fetal tissues and placenta. J. Toxicol. Pathol. 16, 223-229.

Accepted November 2, 2005

Available online at www.sciencedirect.com
SCIENCE DIRECT®
Experimental and Molecular Pathology 79 (2005) 272 – 277
Experimental and Molecular Pathology
www.elsevier.com/locate/yexmp

Microarray analysis on Phase II drug metabolizing enzymes expression in pregnant rats after treatment with pregnenolone-16α-carbonitrile or phenobarbital

Noriko Ejiri [a], Kei-ichi Katayama [a], Naoki Kiyosawa [b], Yasuko Baba [a], Kunio Doi [a,*]

[a] *Department of Veterinary Pathology, Graduate School of Agricultural and Life Sciences, The University of Tokyo, 1-1-1 Yayoi, Bunkyo-ku, Tokyo 113-8657, Japan*
[b] *Medicinal Safety Research Labs., Sankyo Co. Ltd., Shizuoka, Japan*

Received 14 July 2005
Available online 11 October 2005

Abstract

We previously reported the expression profiles of 9 cytochrome P450 isozymes (CYPs) proteins and those of 40 CYPs genes in pregnant rat's liver, placenta and fetal liver after treatment with pregnenolone-16α-carbonitrile (PCN) or phenobarbital (PB). This study was carried out focusing on the gene expression profiles of Phase II drug metabolizing enzymes, Glutathione *S*-transferase isozymes (GSTs) and UDP-glycosyltransferase isozymes (UDPGTs). Fischer 344 (F344) pregnant rats were daily treated intraperitoneally with 50 mg/kg of PCN or 80 mg/kg of PB from 13 to 16 days of gestation (DG). They were sacrificed on 17 DG, and microarray analysis using Affymetrix Rat Expression Array 230 A was performed. Among 16 GSTs genes examined in this study, 7 genes were significantly induced in dam's liver and 3 genes in fetal liver, respectively, in the PCN-group, while 8 genes were significantly induced in dam's liver and 1 gene in fetal liver, respectively, in the PB-group. On the other hand, among 11 UDPGTs genes examined, 5 genes were significantly induced in dam's liver and 3 genes in fetal liver, respectively, in the PCN-group, while 5 genes were significantly induced in dam's liver and 1 gene in fetal liver, respectively, in the PB-group. There were no significant changes in the placenta of all groups. This is the first report of the gene expression profiles of Phase II drug metabolizing enzymes in pregnant rat and fetal livers and placenta after treatment with typical inducers of drug metabolizing enzymes.

Keywords: GSTs; Microarray analysis; Pregnenolone-16α-carbonitrile (PCN); Phenobarbital; Pregnant rat; UDPGTs

Introduction

There are two steps for drug metabolism; Phase I and Phase II reactions. Cytochrome P450 isozymes (CYPs) are one of the representative enzymes in Phase I reaction. Previously, we reported that CYP3A1 was detected in rat placenta through pregnancy (Ejiri et al., 2001). After that, we examined the induction of CYPs proteins in pregnant rat liver, placenta and fetal liver by Western blot analysis and immunohistochemistry using commercially available antibodies against nine CYPs after treatment with pregnenolone-16α-carbonitrile (PCN), dexamethasone (DEX) and phenobarbital (PB) (Ejiri et al., 2003, 2005b). As a result, CYP3A1 protein was induced by PCN and DEX in dam's and fetal livers, with no prominent induction in the placenta (Ejiri et al., 2003). In addition, after PB injection, CYP3A1 protein was significantly induced, CYP2B1 protein was detected and CYP2D1 protein was reduced in dam's liver, and CYP3A1 and CYP2C6 proteins were induced in fetal liver (Ejiri et al., 2005b). In the placenta, no significant induction of CYPs was observed after PB treatment. After those studies, using DNA microarray method, we examined the gene expressions of CYPs in dam's liver, placenta and fetal liver after treatment with PCN and PB (Ejiri et al., 2005a). Ten genes expression significantly increased in dam's liver in the PCN-group, and seven genes expression in the PB-group, respectively. On the other hand, four genes expression increased in fetal liver in the PCN-group, and three genes in the PB-group, respectively. Being common to dam's and fetal livers, the gene expression of CYP3A subfamily and CYP2E subfamily increased in both PCN and PB-groups. In the placenta, only Cyp3A1 gene expression was significantly induced in the PB-

* Corresponding author. Fax: +81 3 5841 8185.
E-mail address: akunio@mail.ecc.u-tokyo.ac.jp (K. Doi).

0014-4800/$ - see front matter © 2005 Elsevier Inc. All rights reserved.
doi:10.1016/j.yexmp.2005.08.002

group, and it also showed a tendency to increase in the PCN-group (Ejiri et al., 2005a).

In this study, we carried out DNA microarray analysis focusing on the expression of Phase II drug metabolizing enzymes, especially Glutathione *S*-transferase isozymes (GSTs) and UDP-glycosyltransferase isozymes (UDPGTs), in dam's liver, placenta and fetal liver after treatment with PCN and PB. Both PB and PCN are known to induce not only CYPs but also GSTs and UDPGTs (Bulera et al., 2001; Longueville et al., 2002; Parkinson, 1996). The protocol of this study was approved by the Animal Care and Use Committee of Graduate School of Agricultural and Life Science, The University of Tokyo.

Materials and methods

Animals

Twelve pregnant rats of the Fischer 344 (F344) strain were purchased from Saitama Experimental Animal Co. (Saitama, Japan). The animals were individually housed in plastic cages in an animal room under controlled conditions (temperature: 23 ± 2°C; relative humidity: 55 ± 5%; light/dark cycle: 14/10 h), and fed commercial pellets (MF, Oriental Yeast Co., Ltd., Tokyo, Japan) and tap water ad libitum. The day of a vaginal plug being recognized was designated as 0 day of gestation (0 DG).

Chemicals

Pregnenolone-16α-carbonitrile (PCN) was purchased from Sigma Chemical Co. (St. Louis, MO), and phenobarbital sodium (PB) and corn oil from Wako Pure Chemical Industries, Ltd. (Tokyo, Japan). PCN was dissolved in corn oil and PB was dissolved in physiological saline immediately before use, and the concentration was adjusted to 50 mg/ml for PCN and 80 mg/ml for PB, respectively.

Treatments

From 13 to 16 DG, 3 dams were daily treated intraperitoneally with 50 mg/kg of PCN (PCN-group), 3 dams with 80 mg/kg of PB (PB-group), 3 dams with 0.1 ml/kg of corn oil alone (CO-group) as control for PCN-group and 3 dams with 0.1 ml/kg of saline alone (Sa-group) as control for PB-group, respectively. All animals were sacrificed by exsanguination under ether anesthesia on 17 DG.

RNA extraction and microarray analysis

Dam's liver, fetal liver and placenta were cut into slices less than 5 mm thick as soon as possible. Then, the slices were submerged in the RNA*later* RNA Stabilization Reagent. After incubated at 4°C for overnight, samples were stored at −80°C until used. Total RNA was extracted using the RNeasy Mini Kit (QIAGEN Inc., CA, USA) from frozen tissues according to the manufacturer's instructions. Microarray analysis was performed according to the Affymetrix protocol. Briefly, of total RNA, 10 μg was used for cDNA synthesis using the T7-$(dT)_{24}$ primer (Primer sequence: 5′-GGC CAG TGA ATT GTA ATA CGA CTC ACT ATA GGG AGG CGG -$(dT)_{24}$-3′). Following this, biotin-labeled cRNA was synthesized from the cDNA using the Enzo High Yield RNA Transcription Labeling Kit (Enzo Diagnostics, NY, USA). Then 25 μg of biotin-labeled cRNA was fragmented and stored at −20°C until ready to perform hybridization. The hybridization solution was prepared using GeneChip Eukaryotic Hybridization Control Kit (Affymetrix), and was hybridized to the Affymetrix Rat Expression Array 230 A at 45°C for 16 h in GeneChip Hybridization Oven 640 (Affymetrix). The chips were washed and stained using the Fluidics Station (Affymetrix) and scanned with GeneArray Scanner.

Data analysis

The microarray imaging data were analyzed using the Microarray Suite 4.0 (Affymetrix) and Spotfire Pro Version 4.2 program (Spotfire Inc., MA, USA).

Table 1
GST and UDPGT isozymes examined

		Genes	Probe ID	Accession no.
GST	Alpha	Glutathione *S*-transferase Yc1 subunit	1367774_at	NM_031509
		Glutathione *S*-transferase Yc2 subunit	1371089_at	AA945082
		Glutathione *S*-transferase mRNA	1368180_s_at	NM_017013
		Similar to GLUTATHIONE *S*-TRANSFERASE 8 (GST 8-8)	1372297_at	AI234527
	Mu	Glutathione *S*-transferase, mu 1 (Gstm1)	1386985_at	M28241
		Glutathione *S*-transferase Yb4 gene (GstYb4)	1369921_at	NM_020540
		Glutathione *S*-transferase, mu type 2 (Yb2) (Gstm2)	1370952_at	AI169331
		Glutathione *S*-transferase, mu type 3 (Yb3) (Gstm3)	1387023_at	NM_031154
		Glutathione *S*-transferase, mu 5 (Gstm5)	1370813_at	U86635
	Pi	Glutathione *S*-transferase, pi 1 (Gstp1)	1388122_at	X02904
	Theta	Glutathione *S*-transferase 1 (theta) (Gstt1)	1368354_at	NM_053293
		Glutathione *S*-transferase, theta 2 (Gstt2)	1368409_at	NM_012796
	Kappa	Similar to GTK1 RAT GLUTATHIONE *S*-TRANSFERASE	1398378_at	AI231779
	Unknown	Microsomal glutathione *S*-transferase 3	1388300_at	AA892234
		Microsomal glutathione *S*-transferase 2	1372599_at	BI290559
		Microsomal glutathione *S*-transferase 1 (Mgst1)	1367612_at	NM_134349
UDPGT	UDPGT-1	UDP glycosyltransferase 1 family, polypeptide A1 (Ugt1a1)	1370613_s_at	AF461738
		UDP glycosyltransferase 1 family, polypeptide A1 (Ugt1a1)	1387759_s_at	J02612
	UDPGT-2	UDP glycosyltransferase 2 family, polypeptide A1 (Ugt2a1)	1369850_at	NM_022228
		UDP-glucuronosyltransferase, phenobarbital-inducible form (UDPGTR-2)	1370698_at	M13506
		UDP-glucuronosyltransferase	1370615_at	U27518
		Androsterone UDP-glucuronosyltransferase (Ugt2b2)	1387825_at	NM_031533
		EST	1385247_at	AA858993
		UDP-glucuronosyltransferase mRNA, complete cds	1387955_at	M31109
		UDP-glucuronosyltransferase (UGT2B12)	1368397_at	NM_031980
	UDP-galactose	Ceramide UDP-galactosyltransferase	1368858_at	L21698
		UDP-glucuronosyltransferase 8 (Ugt8)	1368857_at	NM_019276

Table 2
Primer sequences, cycle numbers and annealing temperature

Gene	Sequence		Cycle number			Annealing temperature
			Liver	Fetal liver	Placenta	
GST alpha	Sense	GCATCAAACTCTTCAACATA	21	25	29	55°C
	Antisense	CTCAACTACATCGCCACCAA				
UDPGT-2	Sense	CTGCGGAAAGGTGTTGGTAT	22	25	30	61°C
	Antisense	GGAGAGAAGCGAAGACTGTA				
GAPDH	Sense	GAGTATGTCGTGGAGTCTACTG	22	22	22	58°C
	Antisense	GCTTCACCACCTTCTTGATGTC				

After global normalization was performed in each experimental datum, fold changes (average of signals of treated groups/average of signals of control groups) were calculated. Student's t test or Welch's t test was done. In this study, we picked up the probes focusing on Phase II drug metabolizing enzymes, especially GSTs and UDPGTs (Table 1). Among those isozymes which we examined, probes of which significance level was $P < 0.05$ and Absolute Call was present were picked up.

Reverse transcriptase polymerase chain reaction (RT-PCR) for GST and UDPGT mRNAs

Total RNA was prepared as described above. For RT-PCR analysis, we selected GST alpha and UDPGT-2 genes because they were up-regulated in both dam's liver and fetal liver. PCR was performed with pairs of oligonucleotide primers corresponding to the cDNA sequences of the rat mRNA. PCR was carried out with 1 μl of cDNA sample in a 100 μl reaction mixture containing 50 pM of sense and antisense primers, 1.25 U of rTaq, 10× PCR buffer and dNTP mixture (Takara, Ohtsu, Japan). This was immediately followed by preheating at 95°C for 7 min, denaturation at 95°C for 1 min, annealing for 1 min and extension at 72°C for 1 min using Takara PCR Thermal Cycler SP (Takara). Annealing temperatures and cycle numbers are shown in Table 2. Optimal cycle numbers were determined in a preliminary experiment to ensure that the amplification was in the linear range and not during the plateau phase. PCR products were identified by electrophoresis on 2% agarose gel (Nippon Gene Co. Ltd.) followed by ethidium bromide (Invitrogen) staining. Fluorescent-gel imaging was carried out using an ultraviolet-CCD video system Fas-III (Toyobo, Tokyo, Japan). The relative band density against glyceraldehyde-3-phosphate dehydrogenase (GAPDH) was represented as the mean ± standard deviation (SD) for three dams, and statistical analysis was carried out using Student's t test or Welch's t test.

Results and discussion

As mentioned before, we have reported the expression profiles of 9 CYPs proteins and those of 40 CYPs genes in pregnant rat's liver, placenta and fetal liver after treatment with PCN or PB by Western blot analysis, immunohistochemistry and DNA microarray analysis (Ejiri et al., 2003, 2005a,b). This study was carried out focusing on the gene expression profiles of Phase II drug metabolizing enzymes, GSTs and UDPGTs.

The selected results of microarray analysis on GSTs and UDPGTs in dam's liver, placenta and fetal liver are shown in Tables 3 and 4. Among 16 probes for drug metabolizing GSTs and 11 probes for UDPGTs, probes showing significant changes in their expression were picked up.

In dam's liver of the PCN-group, the expression of 5 GSTs genes was strongly increased; Glutathione *S*-transferase mu 1 (Gstm1) and Glutathione *S*-transferase mu type 2 (Yb2) (Gstm2) (GST mu class), Glutathione *S*-transferase Yc2 subunit (GST Yc2), Glutathione *S*-transferase (GST) and

Table 3
Gene expression changes of Phase II drug metabolizing enzymes in the dam liver, placenta and fetal liver treated with PCN

		Genes	Fold changes	t test	Accession no.
Dam's liver					
Up-regulated	GST mu	Glutathione *S*-transferase, mu 1 (Gstm1)	8.416	0.000	M28241
		Glutathione *S*-transferase, mu type 2 (Yb2) (Gstm2)	4.482	0.000	AI169331
	GST alpha	Glutathione *S*-transferase Yc1 subunit	1.286	0.020	NM_031509
		Glutathione *S*-transferase Yc2 subunit	6.472	0.001	AA945082
		Glutathione *S*-transferase	3.152	0.000	NM_017013
		Glutathione *S*-transferase 8 (GST 8–8) (CHAIN 8) (GST CLASS-ALPHA)	1.965	0.005	AI234527
	Unknown	Microsomal glutathione *S*-transferase 2	1.943	0.002	BI290559
	UDPGT-1	UDP glycosyltransferase 1 family, polypeptide A1 (Ugt1a1)	3.958	0.000	AF461738
		UDP glycosyltransferase 1 family, polypeptide A1 (Ugt1a1)	4.637	0.000	J02612
	UDPGT-2	UDP glycosyltransferase 2 family, polypeptide A1 (Ugt2a1)	2.472	0.000	NM_022228
		UDP-glucuronosyltransferase, phenobarbital-inducible form (UDPGTR-2)	3.231	0.000	M13506
		UDP-glucuronosyltransferase (UGT2B12)	1.806	0.001	NM_031980
Down-regulated	Unknown	Microsomal glutathione *S*-transferase 3	0.277	0.020	AA892234
Fetal liver					
Up-regulated	GST pi	Glutathione *S*-transferase, pi 1 (Gstp1)	1.469	0.024	X02904
	GST alpha	Glutathione *S*-transferase	4.791	0.018	NM_017013
		Glutathione *S*-transferase 8 (GST 8–8) (CHAIN 8) (GST CLASS-ALPHA)	1.293	0.006	AI234527
	UDPGT-1	UDP glycosyltransferase 1 family, polypeptide A1 (Ugt1a1)	1.437	0.009	AF461738
	UDPGT-2	UDP-glucuronosyltransferase, phenobarbital-inducible form (UDPGTR-2)	2.353	0.002	M13506
		UDP-glucuronosyltransferase (UGT2B12)	1.842	0.000	NM_031980

No significant change was observed in the placenta.

Table 4
Gene expression changes of Phase II drug metabolizing enzymes in the dam liver, placenta and fetal liver treated with PB

		Genes	Fold changes	*t* test	Accession no.
Dam's liver					
Up-regulated	GST mu	Glutathione *S*-transferase, mu 1 (Gstm1)	5.769	0.016	M28241
		Glutathione *S*-transferase, mu type 2 (Yb2) (Gstm2)	2.124	0.001	AI169331
	GST alpha	Glutathione *S*-transferase Yc1 subunit	1.214	0.032	NM_031509
		Glutathione *S*-transferase Yc2 subunit	4.493	0.005	AA945082
		Glutathione *S*-transferase	2.712	0.000	NM_017013
		Glutathione *S*-transferase 8 (GST 8–8) (CHAIN 8) (GST CLASS-ALPHA)	1.516	0.043	AI234527
	GST theta	Glutathione *S*-transferase 1 (theta) (Gstt1)	1.708	0.023	NM_053293
	Unknown	Microsomal glutathione *S*-transferase 2	1.686	0.006	BI290559
	UDPGT-1	UDP glycosyltransferase 1 family, polypeptide A1 (Ugt1a1)	1.654	0.003	AF461738
		UDP glycosyltransferase 1 family, polypeptide A1 (Ugt1a1)	1.704	0.009	J02612
	UDPGT-2	UDP-glucuronosyltransferase, phenobarbital-inducible form (UDPGTR-2)	3.047	0.000	M13506
		UDP-glucuronosyltransferase	1.575	0.043	U27518
		UDP-glucuronosyltransferase (UGT2B12)	1.806	0.001	NM_031980
Fetal liver					
Up-regulated	GST mu	Glutathione *S*-transferase, mu 5 (Gstm5)	1.239	0.025	U86635
	UDPGT-2	UDP-glucuronosyltransferase (UGT2B12)	1.358	0.042	NM_031980

No significant change was observed in the placenta.

Glutathione *S*-transferase 8 (GST 8–8) (GST alpha class) (Table 3). The expression of microsomal Glutathione *S*-transferase 2 was also strongly increased (Table 3). In addition, the expression of Glutathione *S*-transferase Yc1 subunit (GST Yc1) (GST alpha class) showed a slight but significant increase (Table 3). The expression of 5 UDPGTs genes was strongly increased; two probes of UDP glycosyltransferase 1 family polypeptide A1 (Ugt1a1) (UDPGT-1 family), and UDP glycosyltransferase 2 family polypeptide A1 (Ugt2a1), UDP-glucuronosyltransferase phenobarbital-inducible form (UDPGTR-2) and UDP-glucuronosyltransferase (UGT2B12) (UDPGT-2 family) (Table 3). On the other hand, the expression of microsomal Glutathione *S*-transferase 3 was significantly decreased, and there were no UDPGTs genes which were significantly down-regulated (Table 3). In dam's liver of the PB-group, the expression of 7 GSTs genes was strongly increased; Gstm1 and Gstm2 (GST mu class), GST Yc2, GST and GST 8–8 (GST alpha class), Glutathione *S*-transferase 1 (theta) (Gstt1) (GST theta class) and the genes which were similar to microsomal Glutathione *S*-transferase 2 (Table 4). GST Yc1 (GST alpha class) showed a slight but significant increase (Table 4). The expression of 5 UDPGTs genes was strongly increased; two probes of Ugt1a1 (UDPGT-1 family), and UDPGTR-2, UDP-glucuronosyltransferase and UGT2B12 (UDPGT-2 family) (Table 4). On the other hand, there were no GSTs and UDPGTs genes which showed a significant decrease (Table 4).

In the placenta, there were no significant changes in the expression of GSTs and UDPGTs genes in both PCN- and PB-groups (Tables 3 and 4).

In fetal liver of the PCN-group, the expression of GST alpha class, and UDPGTR-2 and UGT2B12 (UDPGT-2 family) was strongly increased (Table 3). The expression of Glutathione *S*-transferase pi 1 (Gstp1) (GST pi family), GST8-8 (GST alpha

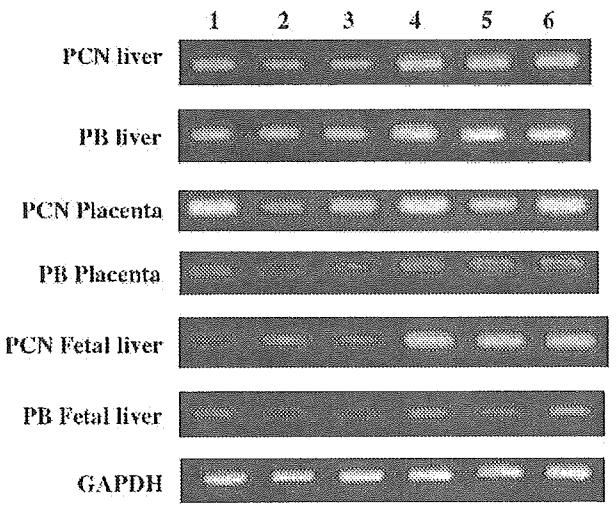

Fig. 1. The expression of GST alpha mRNA by RT-PCR in the dam's liver, fetal liver and placenta. Agarose gel electrophoresis. 1–3: rat number of control group. 4–6: rat number of treated group.

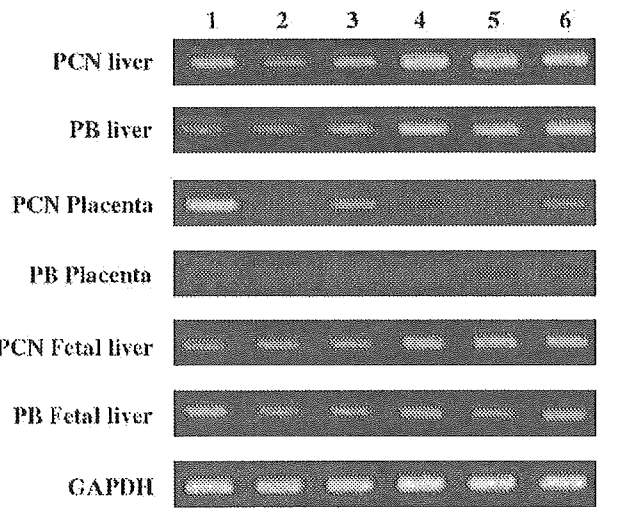

Fig. 2. The expression of UDPGT-2 mRNA by RT-PCR in the dam's liver, placenta and fetal liver. Agarose gel electrophoresis. 1–3: rat number of control group; 4–6: rat number of treated group.

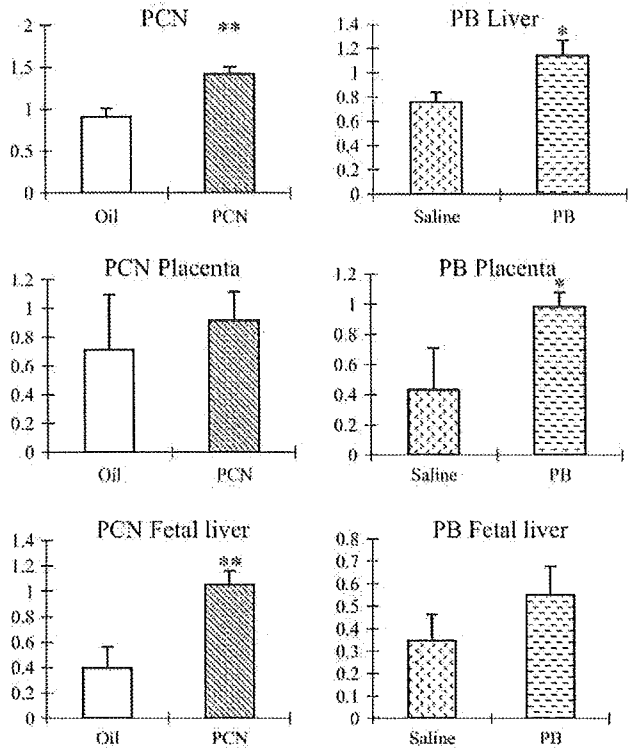

Fig. 3. The relative GST alpha band density to GAPDH by RT-PCR in the dam's liver, placenta and fetal liver. ▭: CO-group; ▨: PCN-group; ▩: Sa-group; ▩: PB-group. $*P < 0.05$ and $**P < 0.01$: significantly different from the control group.

class) and Ugt1a1 (UDPGT-1 family) showed a significant increase (Table 3). On the other hand, there were no GSTs and UDPGTs genes which showed a significant decrease (Table 3). In fetal liver of the PB-group, although no genes showing a remarkable induction, the expression of Glutathione *S*-transferase mu 5 (Gstm5) (GST mu class) and UGT2B12 (UDPGT-2 family) showed a slight but significant increase (Table 4). There were no genes showing decreased expression (Table 4).

As mentioned above, among 16 GSTs genes examined in this study, 7 genes were significantly induced in dam's liver and 3 genes in fetal liver, respectively, in the PCN-group, while 8 genes were significantly induced in dam's liver and 1 gene in fetal liver, respectively, in the PB-group. There were no significant changes in the placenta of both PCN- and PB-groups. On the other hand, among 11 UDPGTs genes examined, 5 genes were significantly induced in dam's liver and 3 genes in fetal liver, respectively, in the PCN-group, while 5 genes were significantly induced in dam's liver and 1 gene in fetal liver, respectively, in the PB-group. There were no significant changes in the placenta of both PCN- and PB-groups. The number of genes showing significant changes in their expression was much larger in dam's liver than in fetal liver, suggesting the difference in profiles of drug metabolizing enzymes between them.

In dam's liver, the expression of GST alpha class was widely induced and that of GST mu class was strongly induced in the PCN-group. In PB-group, the expression of GST alpha and mu classes was mainly induced, and that of GST theta class was also increased. GSTs are arranged into four classes, alpha, mu, pi and theta, based on amino acid identity (Parkinson, 1996). It is said that the members of the alpha and mu classes of GSTs are inducible by PB and corticosteroids (Parkinson, 1996). It was reported in the liver of female rats that GST Ya (GST alpha class) was induced by PB and PCN and GST theta 5 (GST theta class) tended to show an increased expression after PB treatment (Bulera et al., 2001; Longueville et al., 2002). Those reports corresponded well to our present results in the pregnant rat liver. In fetal liver, the expression of GST alpha class was mainly induced in the PCN-group, while only GST mu class was slightly induced in the PB-group.

UDPGTs are classified into two families based on amino acid sequence homology (Kumar and Surapaneni, 2001; Parkinson, 1996). It is said that the PB-inducible UDPGT enzymes and the PCN-inducible UDPGT enzymes are included in UDPGT-1 family, and the enzymes of UDPGT-2 family, especially UDPGT 2B subfamily (forms 2 and 12), are induced by PB (Parkinson, 1996). In the present study, the expression of UDPGT-1 and UDPGT-2 genes was strongly increased in dam's liver in both PCN- and PB-groups. In fetal liver, the enzymes of UDPGT-2 family were induced in both PCN- and PB-groups. UDPGT1a (UDPGT-1 family) is said to be induced by PCN in female rats (Longueville et al., 2002), and, in the present study, UDPGT1a was also strongly induced in dam's liver. In fetal liver, UDPGT1a was significantly but slightly induced in the PCN-group. Although the pi class of GSTs is said to be expressed in the rat placenta (Parkinson, 1996), the significant expression was not observed in the placenta in this study.

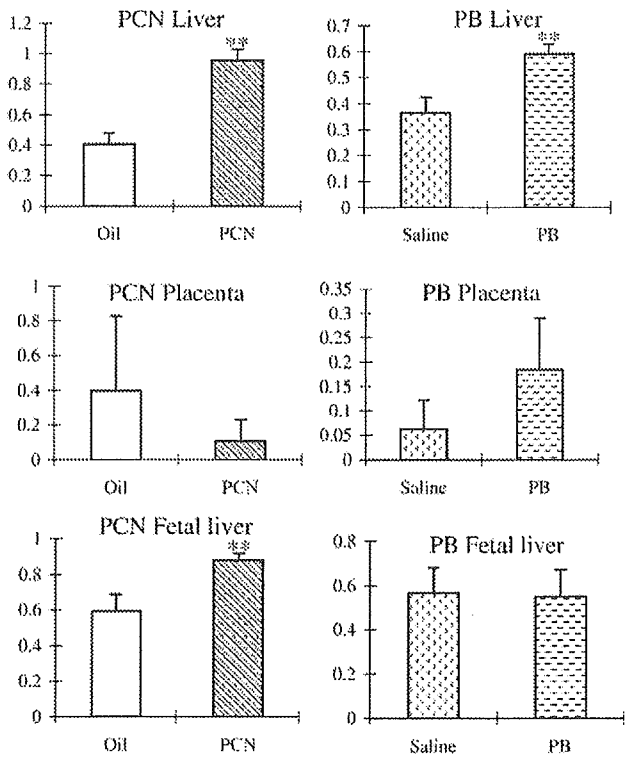

Fig. 4. The relative UDPGT-2 band density to GAPDH by RT-PCR in the dam's liver, placenta and fetal liver. ▭: CO-group; ▨: PCN-group; ▩: Sa-group; ▩: PB-group. $**P < 0.01$: significantly different from the control group.

RT-PCR was performed on GST alpha and UDPGT-2 mRNAs. Those genes were detected to be commonly up-regulated in both dam's liver and fetal liver by DNA microarray analysis.

In dam's liver, the expression of GST alpha and UDPGT-2 mRNAs was significantly elevated in both PCN- and PB-groups (Figs. 1–4).

In the placenta, a significant increase of GST alpha mRNA was observed in the PB-group (Figs. 1 and 3). The expression of UDPGT-2 mRNA did not show a significant change in both PCN- and PB-groups (Figs. 2 and 4).

In fetal liver, the expression of GST alpha and UDPGT-2 mRNAs was significantly elevated in the PCN-group (Figs. 1–4). In the PB-group, the expression of GST alpha and UDPGT-2 mRNAs showed no significant changes (Figs. 1–4).

The results of RT-PCR analysis on the expression of GST alpha and UDPGT-2 in dam's liver were in agreement with those of DNA microarray analysis. In fetal liver, differing from the results of DNA microarray analysis, UDPGT-2 did not show a significant change in the PB-group by RT-PCR. In the placenta, the expression of GST alpha mRNA in the PB-group was a significant but slight change.

In conclusion, this is the first report of the gene expression profiles of Phase II drug metabolizing enzymes in pregnant rats and fetal livers and placenta after treatment with typical inducers of drug metabolizing enzymes.

References

Bulera, S.J., Eddy, S.M., Ferguson, E., Jatkoe, T.A., Reindel, J.F., Bleavins, M.R., Iglesia, F.A., 2001. RNA expression in the early characterization of hepatotoxicants in Wister rats by high-density DNA microarrays. Hepatology 33, 1239–1258.

Ejiri, N., Katayama, K., Nakayama, H., Doi, K., 2001. Expression of cytochrome P450 (CYP) isozymes in rat placenta through pregnancy. Exp. Toxicol. Pathol. 53, 387–391.

Ejiri, N., Katayama, K., Doi, K., 2003. Induction of CYP3A1 by dexamethasone and pregnenolone-16α-carbonitrile in pregnant rat and fetal livers and placenta. Exp. Toxicol. Pathol. 54, 273–279.

Ejiri, N., Katayama, K., Kiyosawa, N., Baba, Y., Doi, K., 2005a. Microarray analysis on CYPs expression in pregnant rats after treatment with pregnenolone-16α-carbonitrile and phenobarbital. Exp. Mol. Pathol. 78, 71–77.

Ejiri, N., Katayama, K., Doi, K., 2005b. Induction of cytochrome P450 isozymes by phenobarbital in pregnant rat and fetal livers and placenta. Exp. Mol. Pathol. 78, 150–155.

Kumar, G.N., Surapaneni, S., 2001. Role of drug metabolism in drug discovery and development. Med. Res. Rev. 21, 397–411.

Longueville, F., Surry, D., Meneses-Lorente, G., Bertholet, V., Talbot, V., Evrard, S., Chandelier, N., Pike, A., Worboys, P., Rasson, JP., Le Bourdelles, B., Remacle, J., 2002. Gene expression profiling of drug metabolism and toxicology markers using a low-density DNA microarray. Biochem. Pharmacol. 64, 137–149.

Parkinson, A., 1996. Biotransformation of xenobiotics. In: Klaassen, C.D. (Ed.), Casarett and Doull's Toxicology: The Basic Science of Poisons, 5th ed. McGraw-Hill Companies, Inc., USA, pp. 113–186.

Available online at www.sciencedirect.com
SCIENCE DIRECT®
ELSEVIER
Experimental and Molecular Pathology 79 (2005) 224 – 228
Experimental and Molecular Pathology
www.elsevier.com/locate/yexmp

Changes in cytochrome P450 isozymes (CYPs) protein levels during lactation in rat liver

Xi Jun He, Noriko Ejiri, Hiroyuki Nakayama, Kunio Doi *

Department of Veterinary Pathology, Graduate School of Agricultural and Life Sciences, The University of Tokyo, 1-1-1 Yayoi, Bunkyo-ku, Tokyo 113-8657, Japan

Received 16 August 2005
Available online 14 October 2005

Abstract

The effects of pregnancy on CYPs protein level in the liver have been investigated in our previous study. Since pregnancy was associated with a decrease in CYPs protein level, the objective of this study was to investigate whether CYPs protein can revert to the virgin control level after delivery. Western blot analysis was performed to investigate the changes of total nine CYPs protein (CYP1A1, CYP2B1/CYP2B2, CYP2C6, CYP2C12, CYP2D1, CYP2D4, CYP2E1, CYP3A1 and CYP4A1) at three distinct phases: delivery (postpartum day 0, PPD 0), peak lactation (PPD 14) and on weaning (PPD 28). By PPD 0, CYP1A1, 2B1, 2B2, 2C6, 2E1 and CYP4A1 were markedly down-regulated when compared with virgin controls. By PPD 14, however, CYP1A1, 2B1, 2B2 and CYP2C6 returned to the virgin control level. All the decreased CYPs during lactation were at the virgin control level at PPD 28. The expression of CYP2C12, CYP2D1 and CYP 3A1 did not differ between lactating, post-lactation and virgin control rats. CYP2D4 was not detectable in microsomal proteins obtained from virgin control rats at a protein loading of 20 μg total protein per lane.

Keywords: CYPs; F344 rat; Western blot analysis; Lactation

Introduction

The cytochrome P450 (CYP) enzyme system is extremely important for the metabolism of xenobiotics as well as endogenous substances, such as fatty acids, prostaglandins and steroids (Lind et al., 2003). Expression of CYP isozymes (CYPs) is also known to be influenced by a variety of endogenous and foreign factors such as inflammation, age, gender, nutritional status, pregnancy and so on. Pregnancy is a physiological state accompanied by a high metabolic demand and an increased requirement for tissue oxygen (Spatling et al., 1992). A body of evidence suggests that pregnancy may be responsible for the depression in the microsomal enzyme activity and the reduction in the total content of CYP in the rat liver (Feuer and Liscio, 1969; Guarino et al., 1969; Neale and Parke, 1973; Dean and Stock, 1975, 1989). We have previously demonstrated that pregnancy is associated with decreased hepatic levels of some CYPs proteins in midpregnancy and/or late pregnancy (He et al., 2005). It has been suggested that changes in the physiological state of an animal may alter CYPs ability to metabolize foreign chemicals (Borlakoglu et al., 1993). The hormonal changes that occur during pregnancy and at the start of lactation are complex, and the balance between the various hormones during lactation is different from that during pregnancy and different again from that in the virgin animal (Smith, 1975). In the lactating animals, milk production introduces an additional metabolic system which competes for the available nutrients with other processes such as the formation of body reserves.

A few studies have been performed on the effects of lactation on tissue metabolism and activities of some enzymes. Smith (1975) has demonstrated that the activities of some enzymes in the rat liver could be influenced by pregnancy and lactation. Based on their observations, Abel et al. (1979) have suggested that drug disposition may be altered during lactation. Review by Williamson (1986) suggests that the main aim of changes in tissue metabolism during rat lactation is to preserve the increased intake of nutrients from diet for milk production. Smith et al. (1998) have demonstrated that major changes in hepatic lipid metabolism must occur to maintain cholesterol homeostasis during rat lactation.

* Corresponding author. Fax: +81 3 5841 8185.
E-mail address: akunio@mail.ecc.u-tokyo.ac.jp (K. Doi).

0014-4800/$ - see front matter © 2005 Elsevier Inc. All rights reserved.
doi:10.1016/j.yexmp.2005.08.009

Table 1
Body and liver weights

Postpartum day (PPD)	Body weight	Liver weight
Virgin control	143.70 ± 1.66	5.78 ± 0.34
PPD 0	156.70 ± 6.61*	7.38 ± 1.17
PPD 14	184.50 ± 5.91***	8.23 ± 0.40**
PPD 28	188.03 ± 17.39*	7.60 ± 1.13

Data are represented as mean ± SD of 6 rats. *$P < 0.05$, **$P < 0.01$, ***$P < 0.001$; significantly different from virgin controls.

It is assumed that, therefore, lactation may also be involved in the regulation of hepatic CYPs expression like pregnancy. Borlakoglu et al. (1993) investigated the alterations of some CYPs in the rat liver during lactation. Western immunoblot analysis of microsomal proteins obtained from pregnant and lactating rats showed that only CYP2C6 and CYP3A1 proteins are expressed at detectable levels, while the expression of others was not detectable in pregnant and lactating rats at a protein loading of 3 μg total protein per well. In their study, comparison was not performed between lactating and virgin control rats. During the past few decades, much less attention has been given to the effect of lactation on the regulation of hepatic CYPs expression. It was therefore of interest to investigate the effect of lactation on the expression of hepatic CYPs proteins. Attention is also paid to some CYPs, which were down-regulated during pregnancy in our previous study, whether and when they could return to the control virgin level. For this purpose, changes in protein levels of nine CYPs in the lactating and post-lactation rat liver were investigated by Western blot analysis at three distinct phases: delivery (postpartum day 0, PPD 0), peak lactation (PPD 14) and on weaning (PPD 28).

Materials and methods

Animals

Twelve pregnant and six age-matched virgin control rats (11 weeks of age) were purchased from Saitama Experimental Animal Co. (Saitama, Japan) and used in this study. The day of delivery recognized was designated as postpartum day 0 (PPD 0). The rats were individually housed in plastic cages in an animal room controlled at 23 ± 2°C and at 55 ± 5% humidity condition with 14 h/10 h light/dark cycle and fed pellets (MF, Oriental Yeast Co., Ltd.,

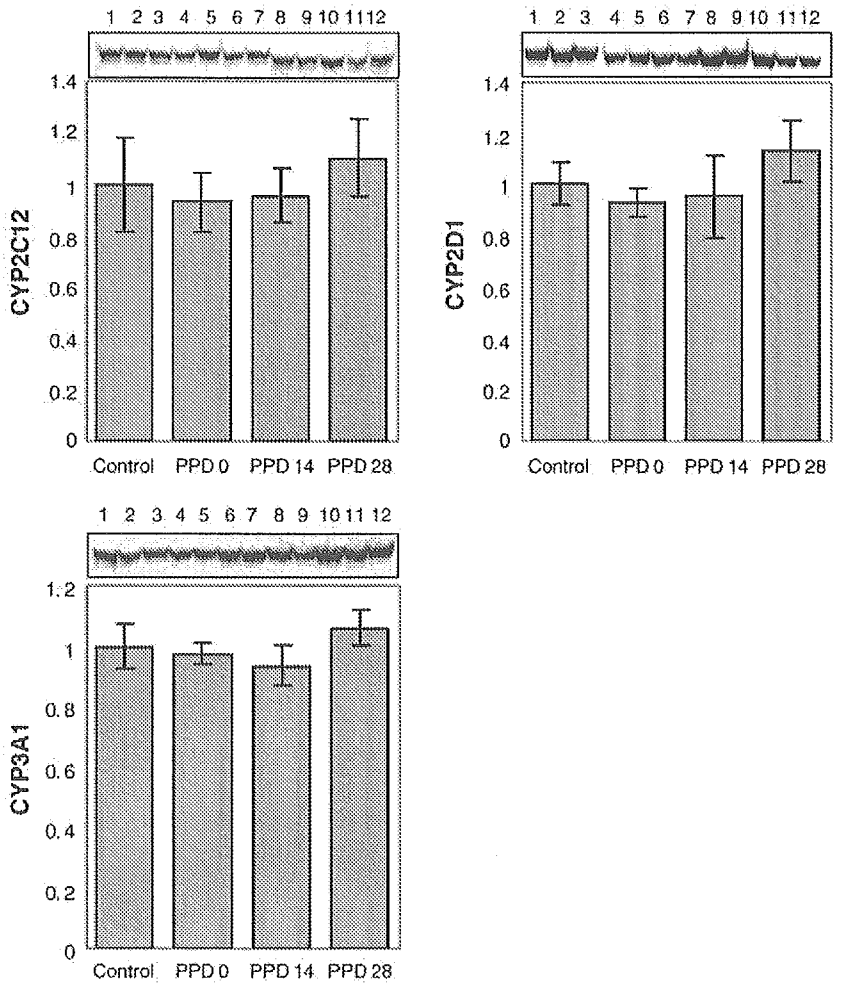

Fig. 1. Western blot analysis of liver microsomes from virgin control, lactating (PPD 0, PPD 14) and post-lactation (PPD 28) rats. The amount of protein per lane was 20 μg (CYP2C12, CYP2D1 and CYP3A1). Lanes 1 to 3: age-matched virgin control rats; lanes 4 to 6: PPD 0 rats; lanes 7 to 9: PPD 14 rats; lanes 10 to 12: PPD 28 rats. Densitometry of Western blotting using monoclonal antibodies against rat hepatic CYP2C12, CYP2D1 and CYP3A1 was performed. Values are expressed as the ratio of lactation (PPD 0 and PPD 14) and post-lactation (PPD 28)/virgin control in arbitrary densitometric units of protein amounts and reported as the means ± SD of 6 rats.

Tokyo, Japan) and water ad libitum. On PPD 0, PPD 14 (peak lactation) and PPD 28 (7 days post-lactation), 6 dams were sacrificed under ether anesthesia, respectively. Livers were removed and used for Western blot analysis. Age-matched virgin rats were used as controls.

Western blot analysis

Livers were homogenized in ice-cold 0.1 M phosphate buffer (PB), pH 7.4, containing 150 mM KCl, 1 mM EDTA Na, 1 mM DTT and microsomes were prepared by differential centrifugation. Briefly, the liver homogenates were centrifuged at 9000 × *g* for 20 min at 4°C, and the resulting supernatant was centrifuged at 105,000 × *g* for 1 h at 4°C. After discarding the supernatant, the pellets were suspended in the same buffer and re-centrifuged. The pellets were re-suspended with 0.1 M PB, pH 7.4, containing 150 mM KCl, 20% glycerol, 1 mM EDTA Na, 1 mM DTT, and stored at −80°C until used. Protein concentration of the samples was measured using bovine serum albumin (BSA) as the standard. Microsomal proteins (20 or 40 μl) were separated using SDS-PAGE in 10% polyacrylamide gels and electrophoretically transferred to polyvinylidene difluoride (PVDF) membrane (Bio-Rad, Richmond, CA), and the plate was blocked with 8% skim milk/TBS for 1 h at room temperature. The membrane was then incubated with the abovementioned anti-rat CYP1A1, CYP2B1/2B2, CYP2C6, CYP2C12, CYP2D1, CYP2D4, CYP2E1, CYP3A1 and CYP4A1 antibodies diluted in 8% skim milk/TBS (1:200) overnight at 4°C followed by another 1 h incubation with horseradish-peroxidase-conjugated secondary antibodies (donkey anti-rabbit IgG; Amersham Pharmacia Biotech Ltd., Arlington Heights IL) and rabbit anti-goat IgG (Cappel, Aurora, OH)). The protein bands were visualized by ECL plus Western blotting detection system (Amersham Pharmacia Biotech Ltd., Arlington Heights, IL) followed by a brief exposure to Hyperfilm (Amersham Biosciences UK Ltd.). Quantity One v3.0 software (PDI, Inc, NY, USA) was used to quantitate the band intensities.

Statistical analysis

Results were presented as the mean ± standard deviation (SD) of six rats. Student's *t* test was employed to calculate the statistical significance between virgin control and postpartum (PPD 0, PPD 14 and PPD 28) groups.

Results

Change in body and liver weights

There were significant increases in the body weights on PPD 0, PPD 14 and PPD 28 compared with virgin controls.

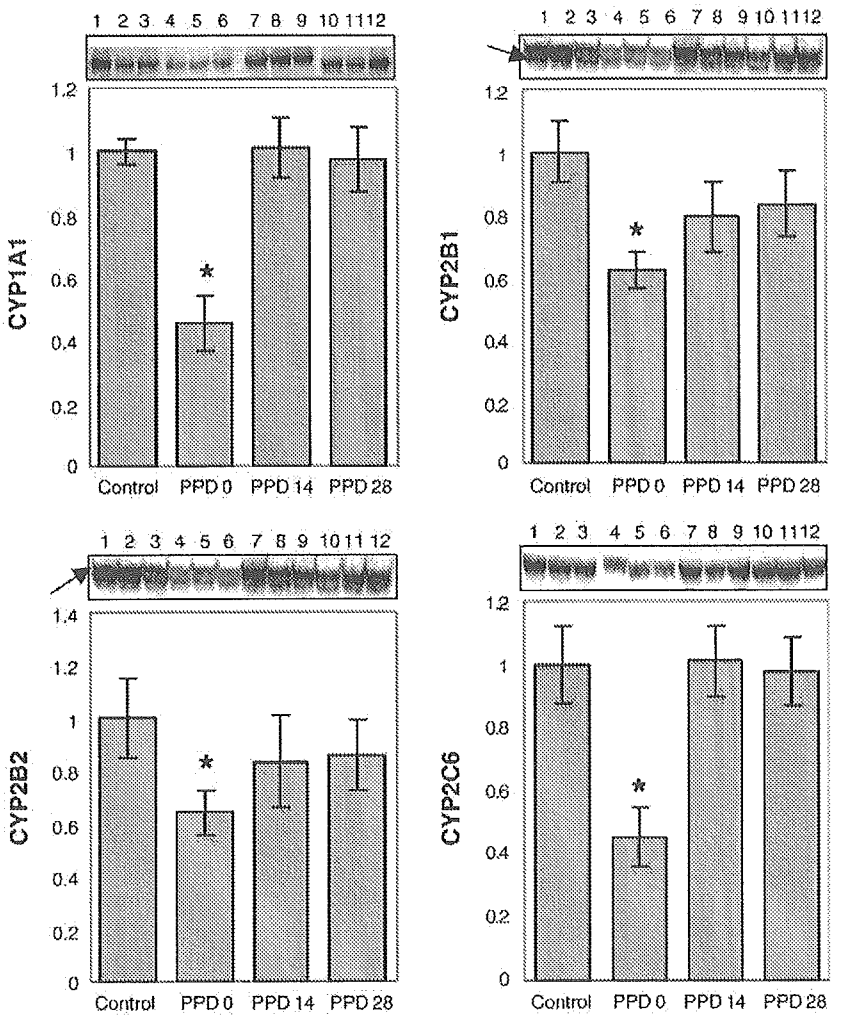

Fig. 2. Western blot analysis of liver microsomes from virgin control, lactating (PPD 0, PPD 14) and post-lactation (PPD 28) rats. The amount of protein per lane was 20 μg (CYP2B1/2 and CYP2C6) and 40 μg (CYP1A1). Lanes 1 to 3: age-matched virgin control rats; lanes 4 to 6: PPD 0 rats; lanes 7 to 9: PPD 14 rats; lanes 10 to 12: PPD 28 rats. Densitometry of Western blotting using monoclonal antibodies against rat hepatic CYP1A1, CYP2B1/2 and CYP2C6 was performed. Values are expressed as the ratio of lactation (PPD 0 and PPD 14) and post-lactation (PPD 28)/virgin control in arbitrary densitometric units of protein amounts and reported as the means ± SD of 6 rats. * Significantly different from virgin controls at $P < 0.05$.

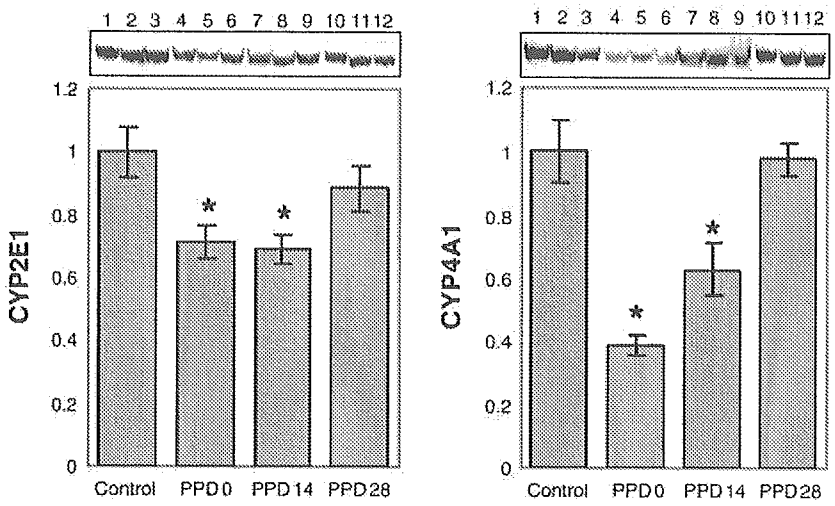

Fig. 3. Western blot analysis of liver microsomes from virgin control, lactating (PPD 0, PPD 14) and post-lactation (PPD 28) rats. The amount of protein per lane was 20 μg (CYP2E1) and 40 μg (CYP4A1). Lanes 1 to 3: age-matched virgin control rats; lanes 4 to 6: PPD 0 rats; lanes 7 to 9: PPD 14 rats; lanes 10 to 12: PPD 28 rats. Densitometry of Western blotting using monoclonal antibodies against rat hepatic CYP2E1 and CYP4A1 was performed. Values are expressed as the ratio of lactation (PPD 0 and PPD 14) and post-lactation (PPD 28)/virgin control in arbitrary densitometric units of protein amounts and reported as the means ± SD of 6 rats. * Significantly different from virgin controls at $P < 0.05$.

However, the increase in body weight was not accompanied with the increase in liver weight when detected on PPD 0 and PPD 28 (Table 1). On PPD 14, there was a significant increase in the liver weight compared with virgin controls (Table 1).

Findings of Western blot analysis

The results of Western blot analysis are shown in Figs. 1–3. The expression of CYP2C12, CYP2D1 and CYP 3A1 proteins did not differ between age-matched virgin control and experimental rats (at PPD 0, PPD 14 and PPD 28) (Fig. 1). CYP2D4 was not detectable in microsomal proteins obtained from virgin controls and experimental animals at a protein loading of 20 μg total protein per lane. Fig. 2 shows significant decreases in the CYP1A1, CYP2B1, CYP2B2 and CYP2C6 contents when detected on postpartum day 0 (45.3%, 61.9%, 63.8% and 45.3% of age-matched virgin control values, respectively). They returned to the virgin control levels by PPD 14 and kept constant levels on PPD 28 (Fig. 2). Decreases in CYP2E1 and CYP4A1 protein levels (71.3% and 39.0% of age-matched virgin control levels) were also found on PPD 0 (Fig. 3), and they were still decreased on PPD 14 (69.3% and 62.3% of virgin control levels). By PPD 28, CYP2E1 and CYP4A1 protein levels returned to virgin control levels.

Discussion

In the present study, in comparison with age-matched virgin control rats, lactating rats showed significantly decreased hepatic levels of six out of nine CYPs proteins (CYP1A1, CYP2B1, CYP2B2, CYP2C6, CYP2E1 and CYP4A1) at day of delivery (PPD 0). By PPD 21 (peak lactation), CYP1A1, CYP2B1, CYP2B2 and CYP2C6 proteins returned to the virgin control levels. All of the hepatic CYPs proteins were at virgin control level at 7 days post-lactation (PPD 28).

We previously demonstrated that pregnancy is associated with decreased hepatic levels of three (CYP2B2, CYP2C6 and CYP4A1) and six CYPs proteins (CYP1A1, CYP2B1, CYP2B2, CYP2C6, CYP2E1 and CYP4A1) in midpregnancy and late pregnancy, respectively. Based on the marked decreases in the same six CYPs proteins at PPD 0, it is obvious that they kept decreased protein levels even though the physiological state has been changes.

In the present study, peak lactation (PPD 14) was linked to an increase in liver weight by up to 42.4%. Although it has been suggested that a decrease in mixed-function oxidase activity during pregnancy is due to a reduction in the hepatocellular capacity to metabolize drugs with an increase in liver size (Symons et al., 1982), it could not be used, however, for interpreting during lactation. Since six CYPs proteins were decreased on PPD 0, not accompanying with an increase in liver weight. Of six decreased CYPs proteins, four returned to the virgin control levels on PPD 14. Based on these observations, it is clear that liver enlargement is not involved in the decrease in CYPs protein during rat lactation.

Progesterone and its metabolites have been suggested to be involved in regulation of activities of the hepatic drug metabolizing enzymes during pregnancy (Feuer, 1979). However, once lactation begins, prolactin is increased, and progesterone is decreased and disappears immediately. Prolactin is essential not only for the initiation of lactation after parturition but also for the maintenance of lactation. In addition to prolactin, successful lactation also requires the hormone oxytocin (Heil and Subramanian, 1998). Dean and Stock (1975) have suggested that lower levels of hepatic microsomal enzyme activity might reflect a biological control mechanism to ensure the elevated levels of progesterone required to maintain the pregnant state. Similarly, down-regulation of CYPs protein probably occurs in response to the hormonal demand for milk production during lactation. In the present study, six out of nine CYPs were down-regulated at